Magnetostrictive nanoparticles in piezoelectric environments for spatially-confined electric brain and nerve stimulation

Title page

Magnetostrictive Nanoparticles in Piezoelectric Environments for Spatially-Confined Electric Brain and Nerve Stimulation

Gabriele Barrera[1]*, Paolo Allia[1] and Paola Tiberto[1]

[1]Advanced Materials Metrology and Life Sciences, INRiM, Strada delleCacce, 91, Turin, 10135, Italy.

*Corresponding author(s). E-mail(s): *g.barrera@inrim.it*

Author Contributions

All authors contributed to the study conception and design. Model definition and data collection were performed by Paolo Allia and Gabriele Barrera. All authors contributed to data analysis and organization. and manuscript The first draft of the manuscript was written by Paolo Allia and Gabriele Barrera and all authors commented on previous versions of the manuscript. All authors read and approved the final manuscript.

Magnetostrictive Nanoparticles in Piezoelectric Environments for Spatially-Confined Electric Brain and Nerve Stimulation

Abstract

Magnetoelectric nanomaterials are investigated in view of their application in noninvasive electrical stimulation of brain cells and nerves for the treatment of neural diseases and pain. The interplay of physical properties in nanoparticles comprised of a magnetostrictive core and a piezoelectric shell is described by modeling the core as a magnetic double-well system with uniaxial anisotropy and the shell as an array of randomly oriented piezoelectric nanocrystals. A careful analysis exploiting the symmetry of magnetic anisotropy allows to calculate the magnetostrictive deformation induced by an ac magnetic field, the resulting electric polarization and the stray electric field of the core-shell structure. An appropriate choice of the core is demonstrated to be crucial in eliciting a strong magnetoelectric response. Dispersing core-shell nanoparticles in a target tissue induces a time-dependent electric field which is always parallel to the magnetic field, permitting the directional stimulation of brain cells. Further, the properties of a magnetoelectric nanocomposite obtained dispersing bare magnetostrictive nanoparticles in a piezoelectric polymer film are investigated. It is shown that the nanocomposite submitted to an ac magnetic field generates an electric field of proper amplitude and can be used as a single flexible electrode for electrical stimulation of nerves in local analgesia.

Keywords: magnetoelectric nanomaterials, core-shell nanoparticles, magnetostriction, piezoelectricity, electric brain stimulation, electric nerve stimulation

1 Introduction

Many basic functions in the human body (cognitive, behavioural, related to motor control) are regulated by the action of transient electric fields or potentials, mostly at a microscopic scale [1–3]. Dysfunctional regulation of native electrical signals brings about serious diseases inducing personal discomfort and having social impact, such as Parkinson's disease, epilepsy, essential tremor, dystonia, Tourette syndrome, obsessive-compulsive disorder [4–7].

As a consequence of the rapid evolution of medicine-oriented technology and the increasing demand for wealth, in the last decades the medical practice has been focused on the development of techniques devised to stimulate either brain cells or nerve endings through electric fields of suitable amplitude, range and frequency, capable to induce a triggering and/or regulating effect on the dysfunctional transmission of native electrical signals [4, 5, 8–13]. Remarkable attention has also been devoted to the local treatment of muscles and nerves in order to elicit pain inhibitory pathways and local analgesia (pain relief) [14, 15]; in this case techniques of transcutaneous electrostimulation of nerves are exploited [16–18].

Acting on the dysfunctional behaviour of native electric fields or potentials in the brain requires that electrical stimuli be applied to a specific region; deep brain stimulation is actuated using fixed on-site electrode implants [7, 19–21] which necessitate brain surgery, with the contraindications and the patients' discomfort typically associated to an invasive technique [22, 23]. More recently, techniques of non-invasive brain stimulation have been introduced [24–26]. However, in transcranial treatments where the electrodes are placed on the scalp, the electric fields can directly affect activity in cortical regions only; moreover, transcranial treatments often result in limited stimulation effects and in electric fields not easily focused on the target [27].

Recently, an alternative strategy has been devised [28] and is presently the subject of active research. Such an innovative approach makes use of multifunctional nanoparticles which can be placed at a specific target inside the cerebral tissue and activated from a distance [28–32]. Multifunctional nanoparticles may help make a breakthrough in many therapeutic protocols owing to the concurrence of specific features such as high dispersibility, smart targeting, cooperative effects, remote control of their properties [30, 33, 34] which are deemed of particular relevance in many branches of today's nanomedicine and personalized medicine. Neural stimulation based on the action of multifunctional nanoparticles is a largely non-invasive technique, at least on a macroscopic scale. Although biocompatibility and metabolic clearance of these smart particles are still under investigation [35], *in vitro* and *in vivo* studies [29, 36–38] indicate that they have the potential to be used as a tool in advanced therapies. In addition, neural stimulation can be actuated by a wireless transmission of low-frequency signals, and does not induce discomfort in the patient [30, 39]).

The key factors behind the interest for a therapy based on nanoparticles are the ability of some materials to combine multi-functional properties, and the ability of nanoparticles to achieve such a combination at the nanometer scale. In this way, many obstacles typically met using conventional methods can be circumvented: in particular, a controlled, suitably targeted dispersion of functional nanoparticles could allow the operator to precisely reach and effectively cure deep regions of the human brain.

In electrical stimulation of brain cells and nerves, the multifunctional properties of some materials act to produce electric effects in the target tissue at the right

frequency[1] through non-electric actuation. In principle, such a goal can be achieved using different multifunctional materials.

Magnetoelectric multiferroics [40] are characterized by the coexistence of two ferroic properties in the same phase, i.e., ferroelectricity and magnetic ordering, with a strong coupling between them [41]. As a consequence, an electrical response can be produced by magnetic stimulation of a multiferroic. However, these materials are rather difficult to produce on a large scale, so that they are possibly more interesting in fundamental than in application-oriented research. Moreover, the interesting properties of bulk multiferroics, closely related to the symmetries of their atomic lattice, may be degraded by the structural defects typically present in a nanostructured material [42]. This is a major hindrance to widespread application of multiferroics in nanomedicine applied to brain cell stimulation.

A class of multifunctional materials that naturally fits the requirements for use in biomedicine and has attracted considerable attention in recent years are the magnetoelectric (ME) core-shell nanoparticles made by a single nanoparticle of a magnetostrictive material such as a ferrite surrounded by a piezoelectric material (typically barium titanate, BTO) [28, 30, 43, 44]. These nanostructures, whose total size is of the order of 20 - 50 nm, have been prepared in different ways [45]. The magneto-electric effect naturally stems from the interplay between magnetic core and piezoelectric shell [11, 46]. In fact, the spontaneous magnetization in the core can be easily driven by an ac magnetic field of given amplitude and frequency; the change of magnetization brings about a periodic deformation (strain) of the core itself because of the magnetostrictive behaviour of the magnetic material (i.e., the coupling between magnetic and elastic properties). In turn, the strain is transmitted to the piezoelectric shell where it induces a periodic electric polarization of the nanoparticle [47, 48]. As a consequence, each ME particle becomes the pointlike source of a time-dependent electric field in the surrounding medium. When a dispersion of ME nanoparticles is placed in close contact with a brain cell (or group of cells) which is generating an erratic sequence of electric pulses, it can provide periodic electrical stimuli at a frequency suitable to trigger the right sequence of pulses in the dysfunctional cells [28].

The magnetoelectric effect has been demonstrated and measured in many ME core-shell nanoparticles belonging to the ferrite-BTO family [37, 38, 49–53], and the feasibility of a therapeutic practice based on these properties has been discussed [28, 37, 54, 55]; however the available experimental results referring to application-oriented properties of these nanomaterials (mostly obtained so far on ME particles whose core is made of the strongly magnetostrictive cobalt ferrite, $CoFe_2O_4$ [49]) are very scattered [49], indicating that the effect is dependent not only on the structure and composition of the core-shell particle but also on its environment. In fact, a detailed, comprehensive analysis at the nanometric scale of the behaviour of these

[1] Typically, low frequencies (not exceeding a few hundreds of cycles per second) are needed to stimulate brain cells or nerves.

core-shell nanostructures is still lacking, and the real effectiveness of the magnetoelectric conversion is still to be satisfactorily assessed.

The magnetoelectric behaviour of these nanomaterials is strongly influenced by the interplay of physical properties of magnetic cores (magnetization, magnetic anisotropy, magnetostriction) and of piezoelectric shells (elastic properties, polarizability), as well as by the crystal structure of the shells and the quality of the core-shell interface. Such a situation makes it difficult to single out properties or quantities useful to define a benchmark of the magnetoelectric performance of core-shell ME nanoparticles. Therefore, the literature is focused on supporting experimental studies [37, 38, 49–53] by means of specific models of ideal core-shell systems [44, 46, 48] in order to figure out their magnetoelectric properties.

In Section 2 a microscopic model of the magnetoelectric behaviour of core-shell nanoparticles with magnetic ferrite core is proposed. The model is based on an accurate representation of the magnetostrictive effects in a single-domain magnetic core, characterized by uniaxial magnetic anisotropy and pictured as a double-well system, according to a widely accepted description of magnetic nanoparticles (Section 3). Different types of magnetic and magnetostrictive behaviour related to the height of the barrier between energy minima of the double well are explored and discussed in Section 3.1. The effect of the magnetostrictive strain on the piezoelectric shell is studied in Section 4.1 by means of a model describing the shell as an agglomerate of BTO nanocrystals with randomly oriented tetragonal axes. The amplitude of the electric field generated by a single core-shell nanoparticle is analyzed in Section 4.1.1, and the cumulative magnetoelectric effect of a uniform dispersion of identical ME nanoparticles is finally discussed in Section 4.1.2.

An entirely different type of magnetoelectric material with potential applications to noninvasive electrostimulation of nerve endings or muscles is introduced in Section 2 and is discussed in Section 4.2. The considered material is a piezoelectric polymer film containing a dispersion of magnetostrictive nanoparticles. The magnetoelectric response of the nanocomposite is explained in terms of the same underlying physical principles as in the case of core-shell nanoparticles: when the film is submitted to an ac magnetic field of moderate amplitude, magnetostriction brings about a deformation of the embedded nanoparticles that results in a macroscopic strain of the whole piezoelectric polymer film where a uniform electric polarization is induced. The behaviour of the nanocomposite is modeled by taking advantage (with suitable adjustments) of the theoretical treatment developed for core-shell particles. The ME film behaves as a single electrode which can be placed in close contact with a target in a patient's body and exploited to apply a magnetically induced electric stimulation over a large surface of the target.

As a matter of fact, core-shell nanoparticles and piezomagnetic nanocomposites belong to different classes of nanomaterials with respect to structure, functionalities and areas of application. However, they share the same underlying physical processes

and principles, characterized by a strict interrelation among different physical properties at the nanometer scale. This interrelation is at the basis of their promising properties as multifunctional systems.

2 Magnetoelectric Nanomaterials

The magnetoelectric nanomaterials investigated in this paper belong in two main families whose common feature is the magnetostriction of magnetic nanoparticles.

a) Core-shell ME particles are typically made of a magnetostrictive core (cobalt ferrite $CoFe_2O_4$ and to a lesser extent magnetite Fe_3O_4 being among the commonest materials studied so far [49]) surrounded by a piezoelectric shell (typically made of barium titanate $BaTiO_3$, or BTO) [38, 49–51, 53]. Each core-shell nanoparticle generates its own magnetoelectric signal, although biomedical applications typically require the cooperative effect of a large number of nanoparticles, as will be discussed in Section 4.1. As a consequence, the model will take into consideration the ME behaviour of a *single* nanoparticle.

A typical core-shell particle for ME applications can be modeled as in Figure 1, panel *a*; the magnetic core, of diameter D, is supposed to be a single grain of a magnetostrictive material characterized by uniaxial magnetic anisotropy. When the magnetic core is submitted to a magnetic field, three mutually orthogonal reference axes can be defined:

- axis 3 is parallel to the direction of the applied field;
- axis 1 lies in the plane defined by axis 3 and the direction of the easy axis of magnetic anisotropy;
- axis 2 is perpendicular to the (1,3) plane.

In general the easy axis is not parallel to any of these three axes, its direction being characterized by the angles θ ($0 \leq \theta \leq \pi$) and ϕ ($0 \leq \phi \leq \pi$) with respect to the field, as shown in Figure 1, panels *a* and *b*.

The shell of the ME particle (of outer diameter D_{out} and typical thickness not exceeding 10-12 nm) [37, 50, 51] is assumed to contain a number of BTO nanocrystals of similar size, characterized by tetragonal symmetry; in each nanocrystal the (X, Y, Z) axes of the tetragonal cell are oriented at random with respect to the magnetic-core axes $(1, 2, 3)$. The local $Z-$axis (i.e., the tetragonal axis of the BTO structure) is drawn in red in the inset of Figure 1, panel *a*. As a matter of fact, at nanoscale level the structure of the as-synthesized BTO tends to be of cubic or pseudocubic type [56]; however, the cubic-to-tetragonal transformation can be induced in the BTO shell by proper thermal treatments at high temperatures [38].

The core is in a well-defined magnetic regime characterizing its behaviour under the action of a driving field of frequency f applied along axis 3. At room temperature,

a magnetic nanoparticle belongs in one of three distinct regimes defined in Section 3, depending on size and magnetic anisotropy.

b) In a different configuration, bare magnetostrictive nanoparticles are dispersed in a continuous film of a diamagnetic, piezoelectric polymer. In this case the magnetoelectricity is a macroscopic effect which takes place in the whole film, whose electric polarization is switched on not through the action of a mechanical stress but by an ac magnetic field acting on the magnetostrictive nanoparticles. The particles are assumed to be uniformly distributed in the polymer; two ideal cases will be explored:

- easy axis of anisotropy randomly distributed in three dimensions with respect to the macroscopic Cartesian axes of the piezoelectric film (Figure 1, panel *c*);
- easy axis having the same direction in all nanoparticles; the collinear configuration can be achieved by applying a strong magnetic field when the particles are being dispersed in the polymer precursor solution (Figure 1, panel *c*).

The polarization of the piezoelectric film is a systemic effect arising from the cumulative deformation of all nanoparticles.

3 Modelling the magnetostriction behaviour

The following assumptions about the nanoparticles are made:

1. the magnetic particles have spheroidal shape with volume $V = \frac{\pi}{6} D^3$, D being the diameter (in core-shell particles, D is the diameter of the magnetic core); their size is such that the magnetization M is always in the single-domain configuration (i.e., neither domain walls nor closure walls are present) [57];

2. they are characterized by an effective uniaxial magnetic anisotropy [58]; the macrospin approximation [59], good for single-domain, nanosized particles, is used to picture the evolution of the magnetization by effect of temperature and magnetic field;

3. they are homogeneously dispersed in a diamagnetic host material without forming chains or aggregates which would bring about largely unpredictable variations of their basic magnetic properties [60];

4. the particles are noninteracting because in biomedical applications, including magnetic hyperthermia, the nanoparticle concentration is generally low [61]; at any rate, weak dipolar interactions can be accounted for by changing the value of the effective anisotropy constant [62];

5. the magnetic and magnetostrictive parameters (saturation magnetization M_s, effective anisotropy constant K_{eff}, magnetostriction constant λ_s) are considered to

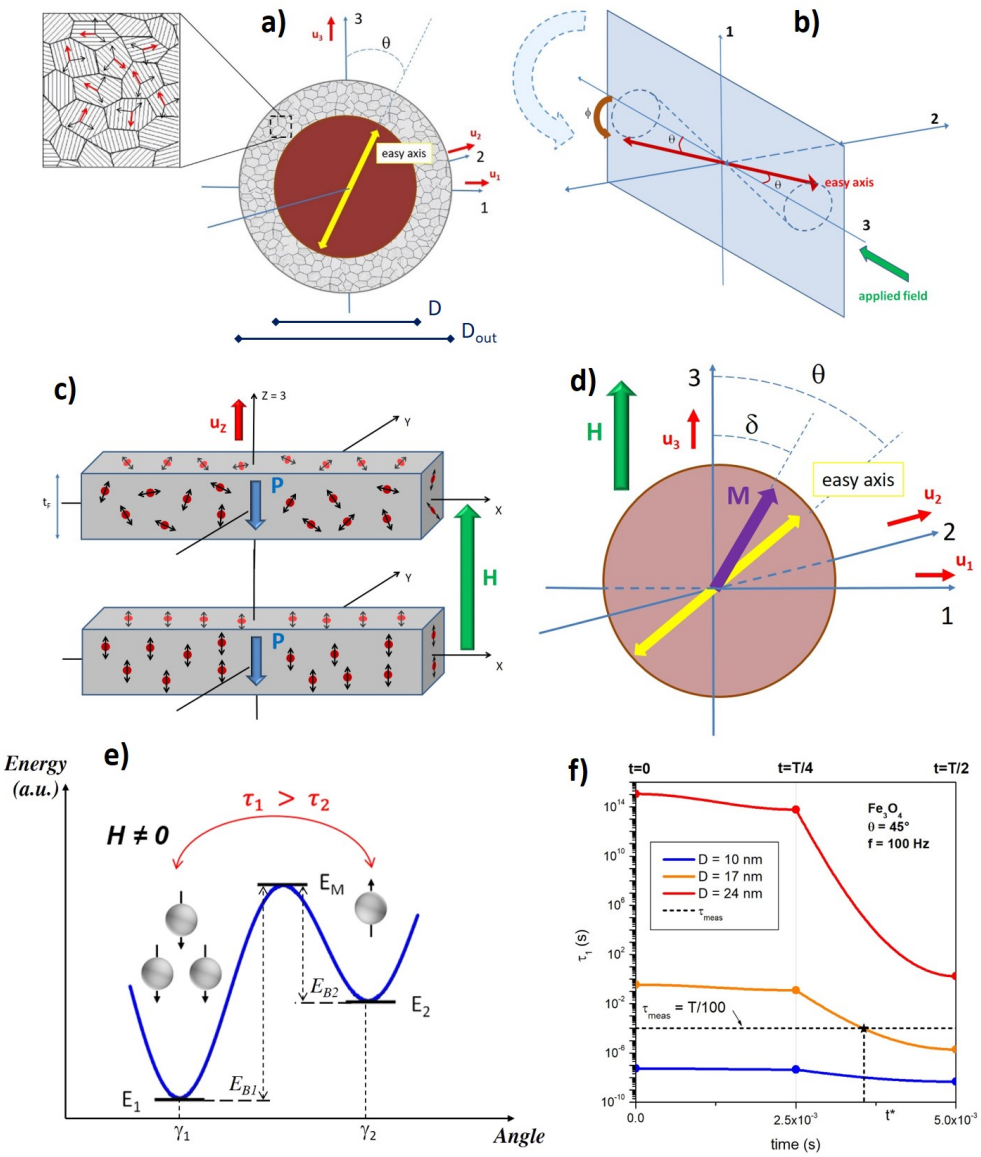

Fig. 1 *a*: Schematic representation of a core-shell ME nanoparticle; *b*: (θ, ϕ) angles defining the easy axis direction with respect to the particle axes and the magnetic field direction; *c*: schematic representation of a piezoelectric polymer containing a dispersion of magnetostrictive nanoparticles with randomly directed easy axes (above) and aligned easy axes (below); *d*: angles and axes in the expression of the magnetostrictive strain (Equation 2); *e*: physical parameters characterizing a DWS; *f*: time behaviour of the parameter τ_1 (escape time from well 1 of the DWS) for magnetite nanoparticles of different sizes (one half-period of the applied magnetic field is considered); the horizontal dashed line indicates the measurement time τ_{meas}.

be independent of particle size and have the representative values given in Table 1;

6. the evolution of magnetization by effect of the ac magnetic field is entirely ascribed to Néel's relaxation, effects arising from Brown's relaxation being excluded from the present treatment; this is an obvious assumption when the particles are embedded in a piezoelectric film; it holds even when they are mostly immobilized by the host tissue during the treatment time, as experimentally checked [63, 64]. On the other hand, it should be noted that a magnetization change arising from pure rotation of the anisotropy axis (i.e., Brown's relaxation) would be ineffective in producing the magnetostrictive strain in the piezoelectric shell that is at the very basis of the effect under study. [2]

A harmonic magnetic field is applied to the magnetic nanoparticles:

$$H(t) = H_V \cos(\omega t) \tag{1}$$

In this work, the maximum amplitude of the driving field is $H_V = 400$ Oe and the frequency is $f = \omega/(2\pi) = 100$ Hz. These values are typical of biomedical applications of core-shell ME nanoparticles for brain stimulation [28, 65].

Table 1 Values of the magnetic and magnetostrictive parameters of magnetite and cobalt ferrite nanoparticles used in this work.

	Fe_3O_4	$CoFe_2O_4$
M_s (emu/cm^3)	350	300
K_{eff} (erg/cm^3)	3×10^5	3×10^6
λ_s	40×10^{-6}	-110×10^{-6}

As an expedient approximation, the strain induced in a magnetic nanoparticle by effect of a variation of its magnetization with respect to the esay anisotropy axis is assumed to depend on a single, magnetization-dependent parameter λ [47] and is a function of the angle between the direction of magnetization and the one along which the strain is observed. The relative elongation (or contraction) $\Delta l/l$ of the particle is evaluated along the direction of the applied field (particle axis 3) as well as along axis 1 and 2. For a particle whose easy axis makes the angle θ with the field one has [57, 66]:

$$\begin{aligned}(\Delta l/l)_3 &= \frac{3}{2}\lambda(M)\left[\cos^2(\theta-\delta) - \frac{1}{3}\right] \\ (\Delta l/l)_1 &= \frac{3}{2}\lambda(M)\left[\sin^2(\theta-\delta) - \frac{1}{3}\right]\end{aligned} \tag{2}$$

[2] In pure Brown's relaxation, the magnetization follows the variation of the magnetic field while remaining stuck to the easy anisotropy axis, without deviating from it; therefore, the magnetic state of the particle is not modified by the field, so that the initial strain of the particle, if any, does not change with time.

$$(\Delta l/l)_2 = -\frac{1}{2}\lambda(M)$$

where δ is the angle between the magnetization and the easy axis, so that the quantity $|\theta - \delta|$ is the angle between magnetization and field (see Figure 1, panel *d*). The form of Equation 2 is related to the fact that the magnetization always lies in the (1,3) plane.

Generally speaking, the isotropic magnetostriction coefficient λ is a monotonic function of M whose maximum (saturation) value is $\lambda_s \equiv \lambda(M = M_s)$. The values of λ_s for both magnetite and cobalt ferrite reported in Table 1 are coincident with the saturation magnetostriction measured in polycrystalline samples with a disordered distribution of crystal directions [57]. When the magnetization process occurs through pure rotations of the magnetization vector without domain-wall displacements, as in the case of single-domain nanoparticles, a quadratic dependence of the magnetostriction coefficient on M is predicted [66]:

$$\lambda(M) = \lambda_s \left(\frac{M}{M_s}\right)^2. \tag{3}$$

In the present case, the relative elongations $(\Delta l/l)_i$ defined in Equation 2 are the diagonal elements of a (3×3) strain tensor $(\Delta l/l)_i \equiv \epsilon_{ii}\,(i = 1, 2, 3)$ whose off-diagonal elements are assumed to be negligible (i.e., the magnetic field is considered not to be a source of shear strain). It can be easily checked that the trace of the ϵ_{ij} tensor is equal to zero, as expected from the requirement of volume conservation [57].

3.1 DWS and Magnetic Regimes

Magnetic nanoparticles characterized by uniaxial magnetic anisotropy are suitably pictured as classical double-well systems (DWS) where the magnetization switches from one energy well to the other one through barrier-crossing transitions [67] (see Figure 1, panel *e*).

The magnetic behaviour of a single nanoparticle is determined by the height of the barrier between wells and by the angles γ_1, γ_2 corresponding to the angular positions of the two energy minima E_1 , E_2; these quantities depend on the anisotropy constant, the particle volume and the applied field H [68]. In the presence of a magnetic field, the energy barriers associated to the two wells are different (see Figure 1, panel *e*), E_{Bi} being the height of the barrier corresponding to the i-th minimum. The corresponding relaxation times are therefore different:

$$\tau_{1,2} = \tau_0 \exp\left(\frac{E_{B1,2}}{k_B T_K}\right) \tag{4}$$

where $\tau_0 \approx 10^{-9}$ s is the reciprocal of the attempt frequency for activated barrier crossing [69] and T_K is the absolute temperature (in this paper, $T_K = 300$ K). When $H = 0$, $E_{B1} = E_{B2} \equiv K_{eff}V$, so that the escape times are equal ($\tau_1 = \tau_2$) and coincident with the Néel's relaxation time τ_N [70, 71]:

$$\tau_N = \tau_0 \exp\left(\frac{K_{eff}V}{k_B T_K}\right) \quad (5)$$

It should be explicitly noted that the problem is complicated by the fact that $E_{B1,2}$ and the time constants $\tau_{1,2}$ generally depend not only on the magnitude of the applied field but also on the angle between the easy axis of the particle and the applied field direction [71].

Three different magnetic regimes can be singled out, resulting from the ratio between the escape time from an energy well and the measurement time. When a driving field of frequency f is applied, the characteristic measurement time is considered to be a small fraction of the field's period T: in fact, it is supposed that during one period of the driving field the magnetization of the nanoparticle is actually assessed a large number of times by the measuring setup, as typical of the experimental practice. In this paper we take $\tau_{meas} = T/100$.

In a thought experiment, the magnetization is assumed to be initially in the well 1 of the DWS (when $t = 0$, $H = +H_V = 400$ Oe); during one period, the particle is assumed to switch from well 1 to well 2 if and only if the escape time τ_1 becomes less than τ_{meas}, i.e., if the energy barrier $E_{B1}(H)$ becomes less than $[\ln(1/f\tau_0)k_B T_K]$ (see Equation 4). Three regimes emerge considering the behaviour of the magnetization over one full period of the applied field:

- when $\tau_1(t = 0) << \tau_{meas}$, the particle is in the superparamagnetic (SP) regime [57] and is labelled as a *S-type particle*. In fact, during one period of the field $\tau_1(t)$ is always lower than $\tau_1(t = 0)$ (see an example in panel *f* of Figure 1, full curve in blue); by symmetry reasons, τ_2 behaves in the same way but for a half-period lag (i,e, $\tau_2(t - \frac{T}{2}) \equiv \tau_1(t)$) so that the magnetization repeatedly switches between the two energy minima during the measurement. In this case, the particle's magnetization is in thermal equilibrium and the $M(H)$ curve is anhysteretic [72] (see Figure 2, panel *a*). Owing to the small nanoparticle diameter, the curvature displayed by the equilibrium $M(H)$ curve in the $-H_V \leq H \leq H_V$ interval is either very small (as in Fe_3O_4) or virtually absent (as in $CoFe_2O_4$);

- in contrast, when $\tau_1(t = \frac{T}{2}) > \tau_{meas}$, the particle is in the blocked anhysteretic regime (*BA-type particle*); the magnetization is never allowed to switch from well 1 to well 2 because the escape time τ_1 is always larger than τ_{meas} (see an example in in panel *f* of Figure 1, full curve in red). In this case, the $M(H)$ curve is entirely determined by the reversible evolution of the γ_i angles with the field and is therefore fully anhysteretic (see the full lines in colour in Figure 4, panel *a*, corresponding to the actual variation of the magnetization when the $H_V = 400$ Oe);

- a case of particular interest is when the $\tau_1(t)$ curve intersects the horizontal τ_{meas} line at some time t^* between $T/4$ and $T/2$; there, the magnetization switches from well 1 to well 2 (see an example in panel *f* of Figure 1, full line in orange). When $t = t^*$ the magnetic field H has a negative value (see Equation 1) and plays

the role of coercive field: $H(t^*) \equiv -H_c$; by symmetry, the magnetization will switch back from well 2 to well 1 at $H = +H_c$ on the return branch. The particle is the blocked hysteretic regime (*BH-type particle*) (see Figure 3, panels *a.1* and *a.2*).

Note that when K_{eff} is constant the key parameter for assigning the particle to one of the three regimes is just the particle diameter D. For magnetite, panel f of Figure 1 shows that nanoparticles with $D = 10$, 17, 24 nm belong in each of the three magnetic regimes and will therefore be taken as representative examples of the three types of nanoparticles. A closely similar analysis for cobalt ferrite (not shown here) indicates that the three magnetic regimes are represented by nanoparticles having diameters $D = 5$, 7, 12 nm.

The magnetic and magnetostrictive behaviour of magnetite and cobalt ferrite nanoparticles belonging in each of the three regimes is discussed in the following Sections.

3.2 Superparamagnetic nanoparticles

In the macrospin approximation, a single magnetic nanoparticle of volume V carries a magnetic moment $\boldsymbol{\mu}$, i.e., it is characterized by a magnetization $\boldsymbol{M}$ of modulus M_s aligned with the easy axis when $H = 0$. In a S-type particle, the result of a thought measurement of the magnetization is a time average of $\boldsymbol{M}$ which makes a very large number of transitions between the two wells during the measurement time τ_{meas}. When $H \neq 0$ the transitions $1 \rightarrow 2$ and $2 \rightarrow 1$ do not have the same probability of occurring because one well is deeper than the other one. An expedient way to estimate this probability is to imagine a set of N fictional replicas of the particle in thermal equilibrium; at a given time the magnetization of $N_1 \leq N$ particles will be in well 1 and the one of $N_2 = (N - N_1)$ particles in well 2; in thermal equilibrium at the temperature T_K, the fractions $n_{1eq} = N_{1eq}/N$ and $n_{2eq} = (1 - n_{1eq})$ are given by the Boltzmann's statistics:

$$n_i = \frac{\exp\left(-\frac{E_i}{k_B T_K}\right)}{\exp\left(-\frac{E_1}{k_B T_K}\right) + \exp\left(-\frac{E_2}{k_B T_K}\right)} \tag{6}$$

where the E_i's are the energy values in the minima of the DWS.

The time average done on *one* S-type nanoparticle during the measurement time τ_{meas} is considered to be equivalent to the instantaneous average over the set of N identical replicas of the particle. In particular, the magnetization is expected to be in well 1 for a time $(n_{1eq}\,\tau_{meas}) \leq \tau_{meas}$ and in well 2 for the complementary time $(n_{2eq}\,\tau_{meas}) = [(1 - n_{1eq})\tau_{meas}]$; the finite time taken by magnetization reversal [71] is considered negligible with respect to τ_{meas}, so that the fast transitions between wells are assumed to occur instantaneously on the time scale considered here [71].

As a consequence, the time average of the particle's magnetization is not equal to zero (for $H \neq 0$) and the particle appears to be magnetized by the applied field. For a

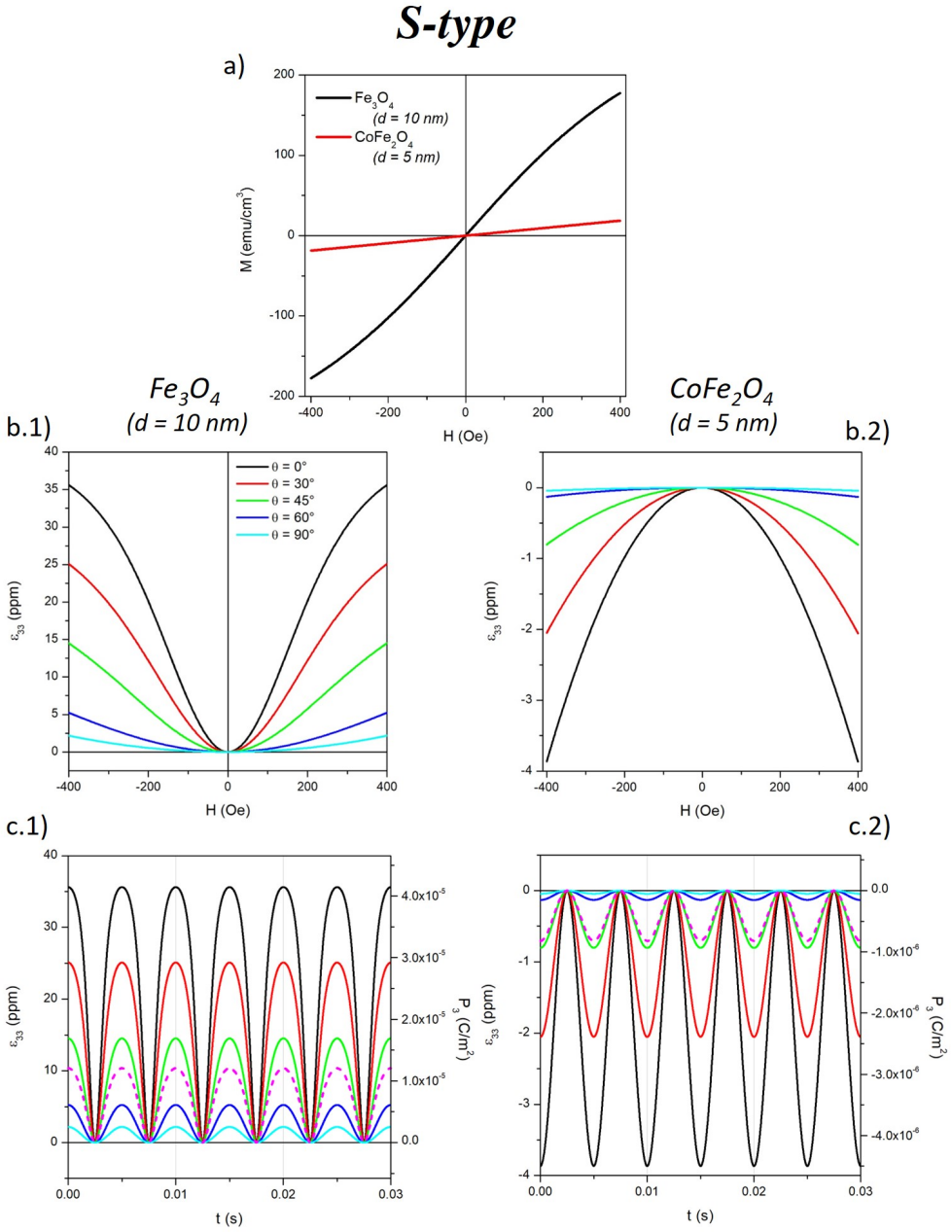

Fig. 2 Magnetic and magnetostrictive properties of typical S-type nanoparticles made of magnetite and cobalt ferrite; *a*: magnetization curves; *b*: magnetostrictive strain ϵ_{33} along the field direction as a function of the instantaneous amplitude of the driving field for various values of the angle θ between the easy axis and the field; *c*: magnetostrictive strain ϵ_{33} of the magnetic core and resulting polarization component $\overline{P}_3$ of a core-shell ME nanoparticle as functions of time (three periods of the driving field are plotted); θ angles as in panel *b.1*.

S-type particle whose easy axis makes an angle θ with the field, it can be shown that the time-averaged magnetization $\overline{\boldsymbol{M}}$ has magnitude:

$$\overline{M} = M_s \left[(n_{1eq} \cos\gamma_1 + n_{2eq} \cos\gamma_2)^2 + (n_{1eq} \sin\gamma_1 + n_{2eq} \sin\gamma_2)^2 \right]^{\frac{1}{2}} \tag{7}$$

where the γ_i's are the angular positions of the two energy minima of the DWS with respect to the easy axis. The $\overline{\boldsymbol{M}}$ vector makes an angle:

$$\delta = \arctan \left[\frac{n_{1eq} \sin\gamma_1 + n_{2eq} \sin\gamma_2}{n_{1eq} \cos\gamma_1 + n_{2eq} \cos\gamma_2} \right] \tag{8}$$

with the easy axis (see the Supplementary Information for a derivation of Equations 7 and 8). It is easy to check that Fe_3O_4 nanoparticles with $D = 10$ nm and $CoFe_2O_4$ nanoparticles with $D = 5$ nm are well within the SP regime; the component of $\overline{\boldsymbol{M}}$ along the field is shown in Figure 2, panel *a* for both materials.

The diagonal elements of the (3×3) strain tensor (ϵ_{ii}) are obtained through Equations 2 and 3, where $M(H) \rightarrow \overline{M}(H)$. The behaviour of ϵ_{33} as a function of H is shown in Figure 2, panels *b.1* and *b.2*, for the two magnetostrictive materials and different θ angles; it can be noted that the magnitude of the strain along axis 3 strongly depends on the angle θ. As expected for S-type particles, the $\epsilon_{33}(H)$ curves are fully anhysteretic; the deformation induced by the field disappears when $H = 0$ because in this case the nanoparticle displays no net time-averaged magnetization. The curves for ϵ_{11} and ϵ_{22} have similar features and are given in the Supplementary Information. The most remarkable difference between the curves for the two materials (apart from the upward/downward curvature arising from the different sign of λ_s, and a minor difference in their shape resulting from the different $M(H)$ curve) is the strong reduction of the magnetostrictive strain in $CoFe_2O_4$ nanoparticles with respect to Fe_3O_4 nanoparticles, in spite of the fact that $|\lambda_s|$ is almost three times larger in cobalt ferrite than in magnetite. In fact, the magnitude of the strain is affected by the barrier between energy wells: the higher is the barrier, the smaller the $(\overline{M}/M_s)$ ratio which determines λ through Equation 3. Owing to the strong difference between the values of K_{eff}, the energy barrier turns out to be higher in 5-nm cobalt ferrite nanoparticles than in 10-nm magnetite nanoparticles.

The $\epsilon_{33}(t)$ waveform is reported in Figure 2, panels *c.1* and *c.2* for three periods of the driving field $H(t)$ (the pertinent scale is on the left vertical axis). The strain has frequency twice that of the driving field, and is in phase with $H(t)$; the waveform appears to be deformed with respect to the sinusoid, particularly in magnetite nanoparticles and for small θ angles. In S-type nanoparticles, the peak-to-peak value of ϵ_{33}, defined as:

$$\Delta\epsilon_{33} = |\epsilon_{33}^{MAX} - \epsilon_{33}^{min}| \tag{9}$$

is highest for $\theta = 0$, i.e., when the easy axis is parallel to the field direction, and decreases with increasing θ. The behaviour of $\Delta\epsilon_{33}$ as a function of θ is shown for both

materials in the Supplementary Information. The average of $\epsilon_{33}(t)$ over all values of θ is given by:

$$\langle \epsilon_{33} \rangle(t) = \frac{1}{2} \int_0^{\pi} \epsilon_{33}(t) \, \sin\theta \, d\theta \tag{10}$$

The result of the average is shown in the same panels as a dashed line (in magenta).

3.3 Magnetically blocked nanoparticles

The cyclic magnetization of single-domain nanoparticles having diameter greater than the critical size for superparamagnetism [57] displays a hysteretic behaviour [68]. In this case, an important role is played by the coercive field H_c^* of the *major* hysteresis loop[3]. For constant temperature and driving-field frequency, the coercive field of a major loop is strongly dependent on nanoparticle size [57].

3.3.1 With magnetic hysteresis

A single BH-type particle is characterized by a symmetrical hysteresis loop with rectangular vertical sides connecting the upper and lower branch and corresponding to the $1 \rightarrow 2$ or $2 \rightarrow 1$ transitions of the magnetization, which take place when τ_1 or τ_2 become less than τ_{meas}, as stated in Section 3.1. A typical example for some values of θ is shown in Figure 3, panels *a.1* and *a.2* for both magnetite and cobalt ferrite nanoparticles. The transitions define the (θ-dependent) coercive field $\pm H_c$ which does not exceed $|H_V|$ in magnitude. Fe_3O_4 nanoparticles with $D = 17$ nm and $CoFe_2O_4$ nanoparticles with $D = 7$ nm belong in this group.

In BH-type particles, the nanoparticle magnetization is not randomly fluctuating in time as in S-type particles; therefore in the upper branch its magnitude is equal to the saturation value M_s, whilst the angle δ between $\boldsymbol{M}$ and the easy axis is equal to γ_1 until the $1 \rightarrow 2$ transition takes place ; there, the angle instantaneously [71] switches to γ_2 (the opposite behaviour takes place on the lower branch).

Therefore, the diagonal elements of the (3×3) strain tensor (ϵ_{ii}) are obtained by using Equation 2 with $\lambda = \lambda_s$. The behaviour of ϵ_{33} as a function of H is shown in Figure 3, panels *b*.1 and *b*.2 for the two magnetostrictive materials and different θ angles; even in this case, the magnitude of the strain along axis 3 strongly depends on the angle θ. As expected for nanoparticles characterized by a well-defined magnetization loop (see panel *a*), the $\epsilon_{33}(H)$ curves generally display a hysteretic behaviour with jumps at $\pm H_c$.

However, the $\epsilon_{33}(H)$ curves do not exhibit hysteresis when the easy axis is both perpendicular and parallel to the field: when $\theta = 90°$, the magnetization entirely results from continuous rotation of $\boldsymbol{M}_s$ towards the field, independently of the energy well where it belongs; when $\theta = 0$, the magnetization reversal does not affect ϵ_{33},

[3] In a major loop the vertex field is such that the magnetization is able to attain the saturation value $\pm M_s$

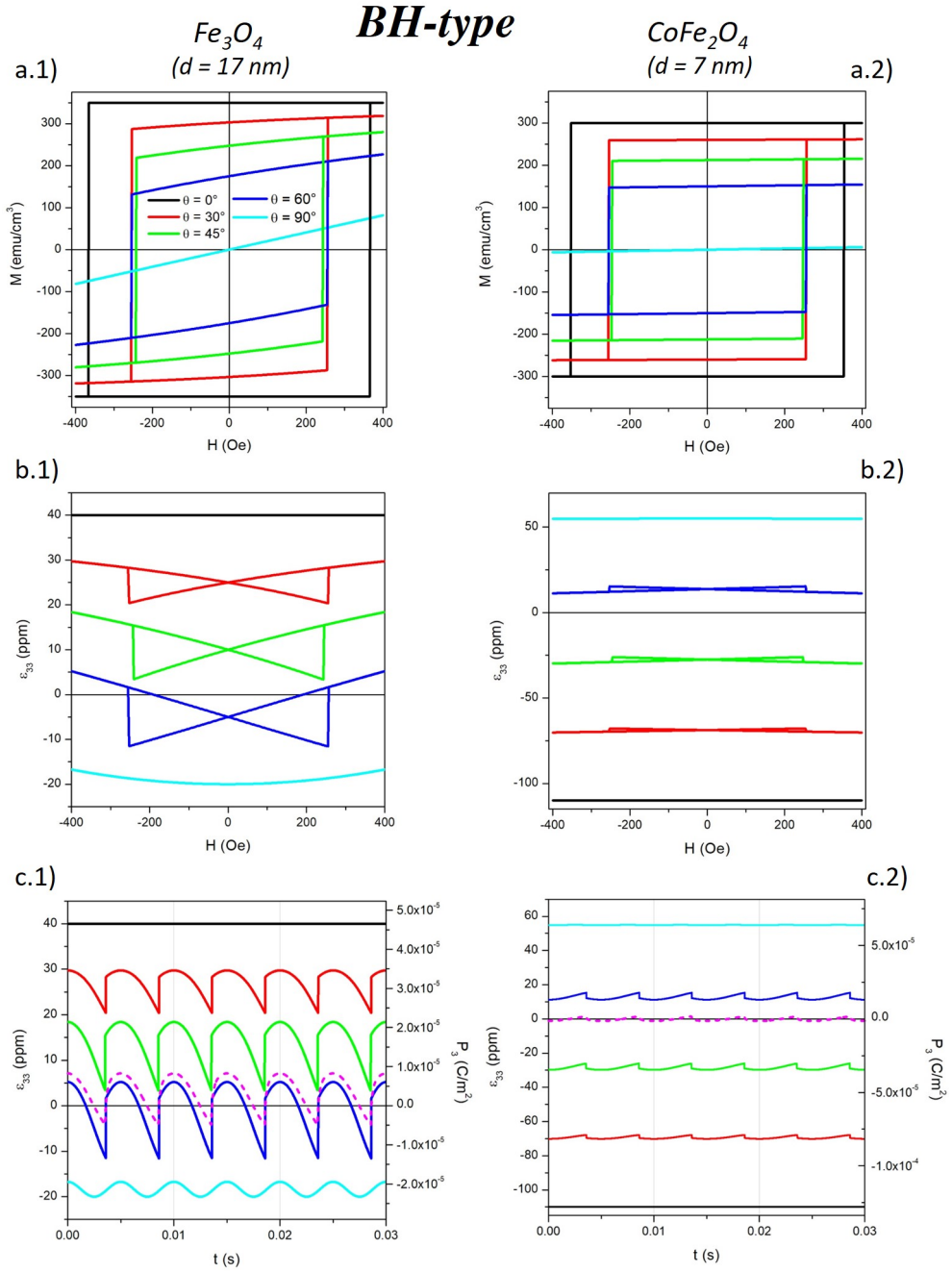

Fig. 3 Magnetic and magnetostrictive properties of typical BH-type nanoparticles made of magnetite and cobalt ferrite; *a*: magnetization curves or various values of the angle θ between the easy axis and the magnetic field; *b*: magnetostrictive strain ϵ_{33} along the field direction as a function of the instantaneous amplitude of the driving field; θ angles as in panel *a.1*; *c*: magnetostrictive strain ϵ_{33} of the magnetic core and resulting polarization component $\overline{P}_3$ of a core-shell ME nanoparticle as functions of time (three periods of the driving field are plotted); θ angles as in panel *a.1*.

the sample's elongation (or contraction) not being modified by the direction of the magnetization vector [66]. The two branches of the ϵ_{33} loop intersect in $H = 0$ where $\epsilon_{33} = \frac{3}{2}\lambda_s(\cos^2\theta - \frac{1}{3})$. The curves for ϵ_{11} have similar features and are given in the Supplementary Information; ϵ_{22} is independent of both H and θ and equal to -2×10^{-5} and 5.5×10^{-5} in Fe_3O_4 and $CoFe_2O_4$ nanoparticles, respectively.

Even in this case, $CoFe_2O_4$ turns out to be definitely less efficient than Fe_3O_4 in producing a large elastic strain along axis 3, because the strong magnetic anisotropy hinders the rotation of the magnetization away from the easy axis. This can be checked by comparing the $\epsilon_{33}(H)$ curves of panels *b*.1 and *b*.2 to the $M(H)$ curves of panel *a* for both materials. It is observed that the magnitude of $\Delta\epsilon_{33}$ is basically determined by the greater or smaller variation of the $M(H)$ curve in the same field interval, which is in turn related to the rotation of the magnetization vector away from the easy axis (such a rotation is almost inhibited in cobalt ferrite particles owing to the large anisotropy energy).

The $\epsilon_{33}(t)$ waveform is shown in Figure 3, panels *c.1* and *c.2*. For $\theta \neq 0$, the periodic strain has frequency twice that of the driving field and markedly differs from a sinusoid, being affected by the jump of ϵ_{33} at the coercive field; when $\theta = 0$, the strain is constant; therefore, a BH particle whose easy axis is parallel to the field is unsuitable in ac applications. In contrast with the behaviour observed in S-type nanoparticles, the peak-to-peak strain $\Delta\epsilon_{33}$ is minimum (and equal to zero) when $\theta = 0$ because the sample's length is not affected by magnetization reversal on the easy axis when this is parallel to the field. $\Delta\epsilon_{33}$ exhibits a maximum at intermediate angles, as shown in the Supplementary Information. The average of $\epsilon_{33}(t)$ over all values of θ (Equation 10) is shown in the same panels by the dashed line (in magenta). In the case of cobalt ferrite, the average curve is barely visible on the scale of Figure 3.

3.3.2 Without magnetic hysteresis

In biomedical applications of ME nanoparticles, the maximum amplitude of the applied field is usually considered to be of the order of a few hundreds of Oe; in large single-domain nanoparticles ($D \gtrapprox 20$ nm for magnetite, $D \gtrapprox 10$ nm for cobalt ferrite) the coercive field of the major loop H_c^* can be significantly larger than H_V; in this case, no $1 \to 2$ transitions are expected to occur by applying a field H between $\pm H_V$ in a particle whose magnetization is initially in well 1. As a consequence, both the magnetic and the magnetostrictive response of BA-type nanoparticles do not display hysteresis. This is made clear in Figure 4, panels *a*.1, *a*.2 and *b*.1, *b*.2 for BA-type nanoparticles of the two materials (Fe_3O_4 nanoparticles with $D = 24$ nm and $CoFe_2O_4$ nanoparticles with $D = 12$ nm belong in this group). For all θ angles, the major loops (black dotted lines) have a coercive field much higher than $|H_V|$, so that when $H(t)$ runs between $+H_V$ and $-H_V$ both the magnetization and the strain only vary on a small portion of the upper branch of the major loop (full lines in colour).

In this case, the magnitude of the magnetization is again equal to M_s and the angle δ between $\boldsymbol{M}_s$ and the easy axis is always equal to γ_1. It should be explicitly noted that the magnetic state described here is by no means an exceptional one: typically, a magnetic nanoparticle not submitted to any magnetic field is at remanence rather than being in the demagnetized state, so that applying an alternate field of amplitude less than H_c makes the magnetization to move back and forth around the remanence value on the upper branch of the major loop.

The resulting $\epsilon_{33(t)}$ waveform is shown in Figure 4, panels *b.1* and *b.2*. As in a BH-type particle, the strain is constant when $\theta = 0$. In contrast with the previous cases, for $\theta \neq 0$ the periodic strain has the same frequency of the driving field. This is related to the peculiar behaviour of both $M(H)$ and $\epsilon_{33}(H)$, which remain on the upper branch of the major loop, as previously discussed. The resulting waveform is more regular than in S-type and BH-type particles. The curves for ϵ_{11} have similar features and are given in the Supplementary Information; ϵ_{22} is independent of both H and θ and equal to -2×10^{-5} and 5.5×10^{-5} in Fe_3O_4 and $CoFe_2O_4$ nanoparticles, respectively.

The peak-to-peak value of the strain ($\Delta\epsilon_{33}$) takes the minimum value (equal to zero) when $\theta = 0$ and displays a maximum at intermediate angles, as shown in the Supplementary Information. The average of the strain waveform over all θ values, done according to Equation 10, is also reported in the same panels (dashed line in magenta).

In analogy with the other cases, the peak-to-peak value of the ϵ_{33} waveforms for all θ angles are very small in single-domain cobalt ferrite nanoparticles, indicating that ME core-shell particles with a $FeCo_2O_4$ core may not be an efficient source of magnetoelectricity, because the advantage of working with a high magnetostriction coefficient is more than counterbalanced by the detrimental effects arising from the large magnetic anisotropy.

4 Magnetoelectric effects

In all regimes described in Sections 3.2 and 3.3, the magnetic field has been shown to produce - to a greater or lesser extent - a deformation ϵ_{ii} along each of the three reference axes i of the magnetic core. The ME effect arising from such a deformation is studied in different ways depending whether the magnetostrictive nanoparticle is surrounded by a BTO shell or embedded in a piezoelectric film. Clearly, the magnetoelectric behaviour of both types of materials depends on the elastic properties of the piezoelectric media surrounding the magnetostrictive nanoparticles. However, a central role is played by the quality of the transmission of the elastic strain from the magnetic nanoparticles to the surrounding elastic medium, that depends on how the materials match at the interface. In this work, it is assumed that the strain is effectively transmitted by ideally matching materials, without interface defects which would attenuate the ME signal.

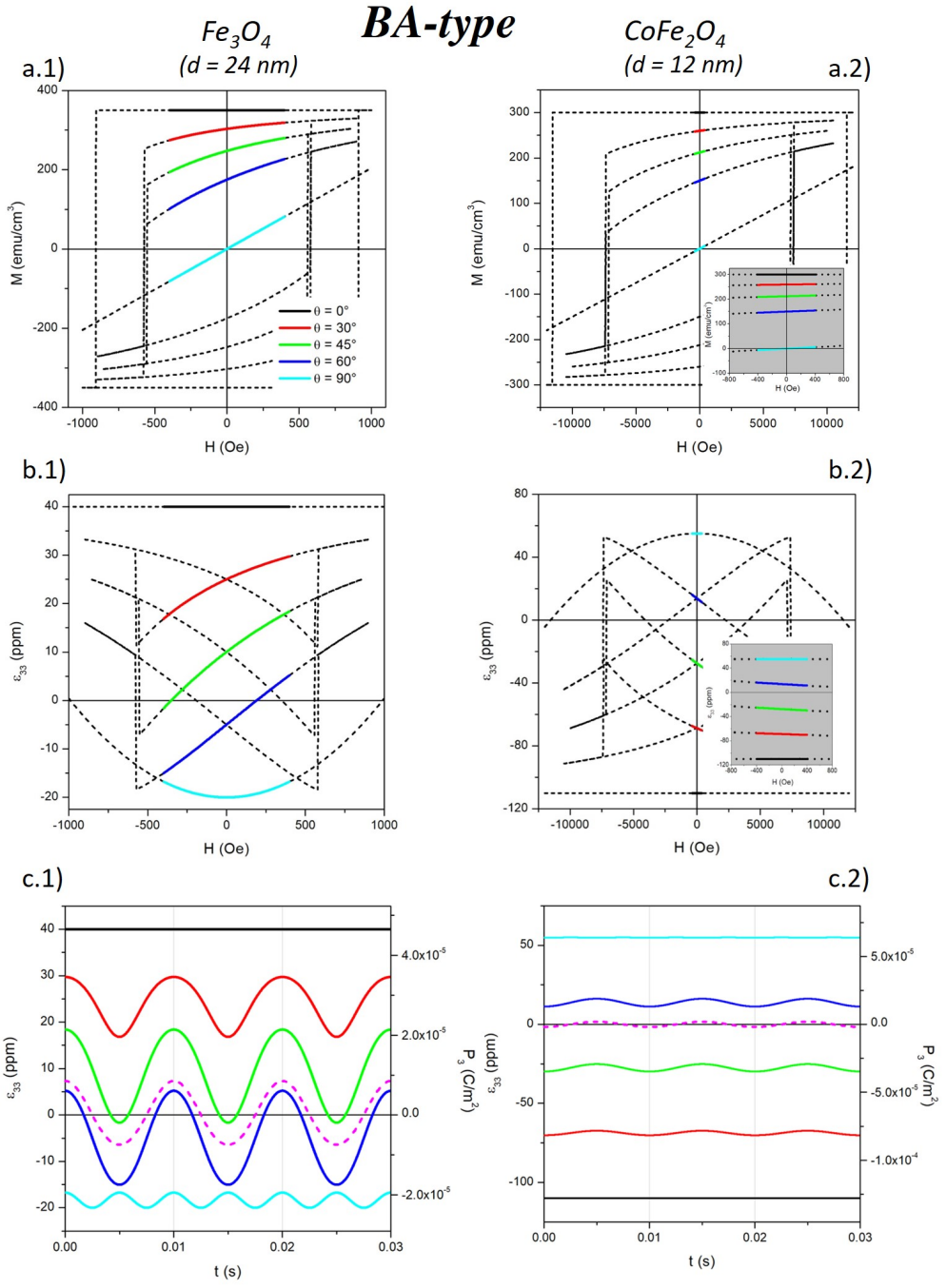

Fig. 4 Magnetic and magnetostrictive properties of typical BA-type nanoparticles made of magnetite and cobalt ferrite; *a*: full lines in colour: magnetization curves or various values of the angle θ between the easy axis and the magnetic field (the dotted lines show the major hysteresis loops; the inset of panel *b*.2 shows a magnification of the region around $H = 0$); *b*: full lines in colour: magnetostrictive strain ϵ_{33} along the field direction as a function of the instantaneous amplitude of the driving field (the dotted lines show the major hysteresis loops; the inset of panel *b*.2 shows a magnification of the region around $H = 0$); θ angles as in panel *a.1*; *c*: magnetostrictive strain ϵ_{33} of the magnetic core and resulting polarization component $\overline{P}_3$ of a core-shell ME nanoparticle as functions of time (three periods of the driving field are plotted); θ angles as in panel *a.1*.

4.1 Core-shell particles

4.1.1 Properties of a single core-shell particle

In a single core-shell nanoparticle whose easy axis makes an angle θ with the magnetic field direction, the deformation of the core produces a polarization of the BTO shell along each of the three particle axes $(1, 2, 3)$, as discussed in the Appendix A.1 where it is shown that the polarization vectors along the three particle axes depend on the time-dependent magnetostrictive strain along axis 3 only, and can be written as:

$$\begin{aligned} \boldsymbol{P}_1(t) &= \overline{P}_1(t)\,\boldsymbol{u}_1 = \frac{1}{3}A\epsilon_3(t)\,\boldsymbol{u}_1 \\ \boldsymbol{P}_2(t) &= \overline{P}_2(t)\,\boldsymbol{u}_2 = \frac{1}{3}A\epsilon_3(t)\,\boldsymbol{u}_2 \\ \boldsymbol{P}_3(t) &= \overline{P}_3(t)\,\boldsymbol{u}_3 = \frac{1}{3}B\epsilon_3(t)\,\boldsymbol{u}_3 \end{aligned} \tag{11}$$

where $\epsilon_3(t) \equiv \epsilon_{33}(t)$ and the $\boldsymbol{u}_i$'s are unit vectors along the particle axes (see Figure 1, panel *a*); the values of the A, B constants (which depend on the piezoelectric shell but not on the magnetostrictive core) are given in the Appendix A.1. It should be noted that the magnetostrictive strain along axis 3 depends on the angle θ for all magnetic regimes. As it turns out, the polarization vectors along axis 1 and 2 have equal magnitude at all times; in BTO B is a positive quantity whilst A is negative, so that the polarization along axis 3 of the particle has different sign with respect to the polarization along the two other axes.

The behaviour of $\overline{P}_3(t)$ with time is just proportional to the one already shown for the $\epsilon_3(t)$ strain in panels *b*.1, *b*.2 of Figures 2- 4 for the three types of nanoparticles and for the two considered materials (in this case, the relevant scale is reported on the vertical axis to the right). The $\overline{P}_1(t) \equiv \overline{P}_2(t)$ waveforms are given in the Supplementary Information.

All polarization components along the particle axes oscillate in phase, so that the total polarization displayed by the ME nanoparticle $\boldsymbol{P}(t) = \Sigma_i \boldsymbol{P}_i(t)$ is a vector whose direction is fixed in space. $\boldsymbol{P}(t)$ makes equal angles with particle axes 1 and 2, and is tilted by an angle $\tilde{\theta}_T$ from the field's direction (axis 3); the angle of tilt, not be confused with the angle θ between the easy axis and the field, is:

$$\tilde{\theta}_T = \arccos \frac{B}{\sqrt{4A^2 + B^2}} \tag{12}$$

With the values given in Table 2, it turns out that $\tilde{\theta}_T \approx 65°$. The angle of tilt is always the same, independently of the value of the angle θ between the easy axis and the field direction. Using the simple model of a dielectric sphere with uniform polarization surrounded by a medium of relative permittivity ϵ_r, the electric field inside the particle is [73] :

$$\boldsymbol{E_i}(t) = -\frac{\boldsymbol{P}(t)}{(2+\epsilon_r)\epsilon_0} \tag{13}$$

which obviously reduces to the usual expression $\boldsymbol{E} = -\boldsymbol{P}/3\epsilon_0$ when $\epsilon_r = 1$. The peak-to-peak value of the magnitude of the electric field is

$$\Delta E_i = \frac{1}{3(2+\epsilon_r)\epsilon_0}\sqrt{4A^2+B^2}\,\Delta\epsilon_3 \tag{14}$$

where $\Delta\epsilon_3 \equiv \Delta\epsilon_{33}$ was defined in Equation 9. The maximum value of the alternating voltage at the surface of a ME core-shell nanoparticle with outer diameter D_{out} is just the product $(\Delta E_i\, D_{out})$.

Considering a standalone ME nanoparticle embedded in a medium with $\epsilon_r \approx 1$, and using the values of Table A1 one gets $\Delta E_i \approx 1.04 \times 10^{11}\,\Delta\epsilon_3$.

As an example, in a ME nanoparticle with a S-type magnetite core with $\theta = 45°$, $\Delta E_i \approx 1.56 \times 10^6$ V/m; taking $D_{out} \approx 30$ nm [37] the maximum voltage across the nanoparticle is expected to be $\Delta V \approx 47$ mV.

In the case of a ME nanoparticle with S-type cobalt ferrite core surrounded by a medium with $\epsilon_r \approx 1$, the following values are calculated when $D_{out} \approx 30$ nm and $\theta = 45°$: $\Delta E_i \approx 1.04 \times 10^5$ V/m, $\Delta V \approx 3$ mV. These values are in agreement with the ones obtained on ME nanoparticles with ferrite cobalt cores using a different modeling approach [11] which has recently been validated by *in-vivo* measurements.

The electric field $\boldsymbol{E}_o$ outside the nanoparticle behaves as a dipole field [74]; an estimate of its peak-to-peak value at a distance $d > D_{out}/2$ from the center of the nanoparticle is obtained by making the average of $|\boldsymbol{E}_o|$ over the spherical surface of radius d:

$$\overline{\Delta E_o} = 1.38\,\Delta E_i \left(\frac{D_{out}}{2d}\right)^3 \tag{15}$$

A suitable parameter used to measure the efficiency of magnetoelectric conversion of core-shell nanoparticles is the mean magnetoelectric coefficient $\overline{\alpha}_{ME} = \Delta E_i/\Delta H$, where ΔH is the change of magnetic field needed to obtain the peak-to-peak value ΔE_i of the internal field. In our case, $\Delta H = H_V$ because one half-period of the driving field is enough to get ΔE_i (see panel *c* of Figures 2 - 4). As a matter of fact, a wide variety of values of the $\overline{\alpha}_{ME}$ coefficient have been measured [49–51], suggesting that this parameter is influenced by the intrinsic properties of the core-shell structure and by the nature of the particle's environment.

The electric field inside the nanoparticle is affected by the relative permittivity of the surrounding medium (Equation 14); as a consequence, the product

$[(2+\epsilon_r)\,\overline{\alpha}_{ME}]$, which is independent of the external medium, is a more appropriate parameter to characterize the magnetoelectric response of the nanoparticle. The permittivity-independent coefficient is defined as:

$$[(2+\epsilon_r)\,\overline{\alpha}_{ME}] = \frac{1}{3\epsilon_0}\sqrt{4A^2+B^2}\,\frac{\Delta\epsilon_3}{H_V} \tag{16}$$

Typical values of this quantity are reported in Table 2 for three types of magnetic cores and the considered materials.

Table 2 Values (in mV/cm/Oe) of the permittivity-independent product $[(2+\epsilon_r)\,\overline{\alpha}_{ME}]$ of core-shell nanoparticles for two magnetostrictive materials and three types of magnetic cores.

Type	Fe_3O_4	$CoFe_2O_4$
S	8.2×10^4	5.4×10^3
BH	8.6×10^4	1.8×10^4
BA	1.1×10^5	2.3×10^4

According to Table 2, when the ME nanoparticles are surrounded by a dielectric medium with $\epsilon_r \approx 1$, the mean magnetoelectric coefficients take values around 3×10^4 in nanoparticles with magnetite core and in the range $2-8\times10^3$ in particles with cobalt ferrite core. These values can be compared with the experimental results obtained on real core-shell ME particles, that range between 2-3 mV/cm/Oe [75] and 1×10^4 mV/cm/Oe [51]. [4] It should be noted that core-shell nanoparticles with $\overline{\alpha}_{ME}$ values closely similar to the results reported in Table 2 have been shown to be effective in inducing electrical stimuli in the brain of mice [30]. On the other hand, even when core-shell particles with significantly smaller $\overline{\alpha}_{ME}$ coefficients were used, stimulation effects in mice were observed as well [29].

It can be concluded that for a given host medium the value of the magnetoelectric coefficient of core-shell nanoparticles with single-domain magnetic cores is strongly affected by the magnetic material (magnetite being favoured with respect to cobalt ferrite), while the type of magnetic regime in the core plays a marginal role, particularly in the case of magnetite. This means that the magnetoelectric performance is not particularly influenced by the size of the magnetic cores, which is an important feature in applications making use of magnetic nanoparticles produced through chemical routes [76], where different magnetic regimes coexist because of a wide distribution of particle sizes. Of course, a crucial role in determining the actual efficiency of core-shell particles is played by the piezoelectric response of the BTO shell, which strongly depends on the quality and the arrangement of the BTO nanocrystals. However, the values reported in Table 2 indicate that the right choice

[4] The large scatter of measured $\overline{\alpha}_{ME}$ values found in the literature is possibly related to the quality of the BTO shell structure and of the core-shell interface.

of the magnetic material has comparable importance.

In living tissues a wide distribution of values of ϵ_r have been measured [77]. The matter is complicated by the fact that reliably estimating the relative permittivity of living tissues al low frequency ($f \leq 10$ kHz) is still a debated issue [78]. According to recent views [78], ϵ_r can be of the order of 1×10^5 in brain (gray matter) at $f = 100$ Hz. In this case, Equations 14 and 15 indicate that in a 30-nm core-shell nanoparticle with a superparamagnetic magnetite core, the internal electric field has value E_i would be of the order of 50 V/m; as a consequence, the field generated by the ME nanoparticle in the tissue would still have a value of more than 0.1 V/m at a distance as large as about 100 nm from its surface. Such an amplitude is sufficient to elicit the response of neurons submitted to repetitive electrical stimuli [79], to activate neuronal networks [8] and to evoke neural spikes [8].

4.1.2 Dispersion of core-shell particles in a dielectric medium

In biomedical applications such as neural stimulation, a large number of identical nanoparticles are needed to produce a significant effect in the living tissue.

In this Section, we propose a simplified model of the electrical stimulation by an uniform dispersion of identical ME nanoparticles. Let us single out a spherical region of diameter D_R inside a dielectric medium with a low-frequency permittivity $\epsilon_r \approx 1 \times 10^5$, i.e., comparable to the one of the cerebral tissues. Let us imagine that the volume of such a sphere is populated by a large number of evenly distributed core-shell nanoparticles of diameter $D_{out} \ll D_R$, fixed in space, and with volume fraction f_V; no particles are instead supposed to be present outside the sphere. Typically, in a particle dispersion there is no way to control the direction of the easy axes of the magnetic cores, so that the nanoparticles are assumed to have randomly distributed easy axes.

In general, the easy axis direction of a magnetic core is characterized by the angle of tilt θ from the magnetic field direction and by the azimuth ϕ around the the same direction, as shown in Figure 1, panel *b*. It should be noted that axis 3 of all nanoparticle cores is always coincident with the magnetic field direction; in contrast, axes 1 and 2 are randomly distributed around the magnetic field direction, so that the (1,3) plane takes all orientations in space. The total electric polarization of the system is obtained by making an average over both θ and ϕ angles of the single-particle polarization vectors $\boldsymbol{P}_i$ defined in Equation 11. It is easily checked that the average over ϕ cancels out the polarization vectors along axes 1 and 2 ($\boldsymbol{P}_1$ and $\boldsymbol{P}_2$) whilst $\boldsymbol{P}_3$ is left unaffected (in fact, $\overline{\boldsymbol{u}}_1 = \overline{\boldsymbol{u}}_2 = 0$, $\overline{\boldsymbol{u}}_3 = \boldsymbol{u}_3$); therefore:

$$\overline{\boldsymbol{P}}_1 = \overline{\boldsymbol{P}}_2 = 0 \quad ; \quad \overline{\boldsymbol{P}}_3 = \boldsymbol{P}_3. \tag{17}$$

The average of $\boldsymbol{P}_3(\theta)$ with respect to the angle θ (denoted by brackets) is done recalling that ϵ_3 is a function of this angle. By definition, $\langle \boldsymbol{P}_3 \rangle = \frac{1}{3} B \langle \epsilon_3 \rangle \, \boldsymbol{u}_3$, where

$\langle \epsilon_3 \rangle$ was defined in Equation 10. The magnitude of $\langle \boldsymbol{P}_3 \rangle$ for all types of ME nanoparticles is shown in Figures 2, 3, and 4 as dashed lines (in magenta; the values are reported on the right axis). Therefore, the whole spherical region may be thought as characterized by a uniform polarization vector $\boldsymbol{P}_{tot} = f_V \langle \boldsymbol{P}_3 \rangle$, which is *parallel* to the magnetic field and oscillates in time.

In other words, a magnetic field $\boldsymbol{H}(t)$ is able to generate in the spherical region a uniform electric field $\boldsymbol{E}(t)$ having the same direction of $\boldsymbol{H}(t)$ because of the presence of dispersed ME nanoparticles. This result paves the way to a user-guided technique of directional neural stimulation in a target region. The magnitude of the uniform electric field inside the sphere is:

$$E_i(t) = \frac{P_{tot}(t)}{(2+\epsilon_r)\epsilon_0} \approx f_V \frac{\langle P_3 \rangle(t)}{\epsilon_r \epsilon_0} \tag{18}$$

Considering core-shell nanoparticles with a S-type magnetite core, one has $\langle P_3 \rangle \approx 1.2 \times 10^{-5}$ C/m^2 (see Figure 2, panel *c.1*), so that $E_i \approx 13.6\, f_V$ V/m everywhere inside the sphere. Therefore, a volume fraction $f_V \approx 7 \times 10^{-3}$ would be enough to generate in the spherical region an electric field larger than the lower neuronal activation threshold in the brain. Equation 18 clearly indicates that the local permittivity of the tissue plays a critical role on the ME response of this material. The ME effect is maximized when the BTO is put in direct contact with the target tissue, as supposed here. Such an assumption is supported by the low toxicity of BTO ceramics [80] that can avoid using a biocompatible coating of the core-shell nanoparticles. Such a coating would partially shield the electric field generated by the nanoparticle, jeopardising the treatment's effectiveness.

4.2 Nanoparticles embedded in a piezoelectric polymer

In ME core-shell structures, each nanoparticle acts as an individual, point-like source of electrical field (or voltage), although significant effects on a target tissue can only be achieved by introducing a suitable dispersion of ME nanoparticles, as discussed in Section 4.1.2. Of course, this is not always the technique of election, particularly in treatments involving large zones of the body surface [14, 17].

In this Section a different strategy will be explored, based on the cumulative effect of magnetic nanoparticles embedded in a piezoelectric polymer. This nanocomposite can used as a single, non-invasive, flexible, reusable electrode which can be directly applied to the target.

Dispersing bare magnetostrictive nanoparticles in a uniaxially oriented film of polyvinylidene fluoride (PVDF) could be an interesting approach. PVDF is a commercial piezoelectric polymer having excellent piezo-, pyro-, and ferroelectric activity and a great potential in different applications [81, 82]. In particular, the β phase of PVDF guarantees an optimal piezoelectric response [83], which is usually stimulated by the action of a mechanical stress [83], resulting in applications such as wearable

tactile sensors or force/pressure sensors [83, 84].

In those cases, the electrical effects produced by the film are a sensitive tool to measure a mechanical disturbance. However, the electrical response of the piezoelectric film is interesting *per se* when the focus is on the electrical stimuli which can be produced in living tissues from an electrical field source placed in close contact with a specific area of a patient's body. It is therefore important to ascertain whether and how much the piezoelectric response of the PVDF film can be stimulated not by the action of a mechanical stress but by the magnetostrictive response of an assembly of embedded magnetostrictive nanoparticles driven by an ac magnetic field. Some measurements have been done on PVDF films filled with magnetite and cobalt ferrite nanoparticles [85, 86] demonstrating the magnetoelectric effect in these nanocomposites.

PVDF films may have rectangular shape with a thickness t_F of the order of a few hundreds of micrometers, while length and width of the film may be of the order of one centimeter (Figure 1, panel *c*). The draw direction of the polymer film [83] defines the X-axis; the Y-axis is perpendicular to the draw direction and lays in the plane of the film and the Z-axis is normal to the plane of the film. The ac magnetic field is applied along the Z-axis; therefore, this direction also corresponds to axis 3 of nanoparticles, as said in Section 2.

In the following analysis, the active magnetic particles are assumed to be superparamagnetic (S-type) and made of magnetite. In Section 4.1.1 it was shown that Fe_3O_4 nanoparticles present a good compromise between a sufficiently high magnetostriction constant and a moderate magnetic anisotropy; moreover, panels *c* of Figures 2, 3, 4 indicate that the magnetostrictive response of S-type magnetite nanoparticles is comparable to the one of magnetically blocked particles, and somewhat easier to treat.

It is assumed that a volume fraction f_V of bare magnetite particles of diameter $D = 10$ nm are uniformly distributed in the polymer matrix. The particles are mechanically immobilized in the film, so that the magnetic behaviour is uniquely determined by Néel's relaxation. Under the action of the driving field, each nanoparticle induces a local deformation in the surrounding piezoelectric film, as described by Equations 2 and 3.

The average distance d_{ave} between the centers of two adjacent nanoparticles of diameter D is:

$$d_{ave} \approx \left(\frac{\pi}{6 f_V}\right)^{1/3} D \tag{19}$$

For very low volume concentrations, d_{ave} can become much larger than the diameter D, thereby preventing the transmission at long distance of the local deformation field generated around each individual nanoparticle. However, when $f_V \approx 0.1$ (a value

such that the mechanical and piezoelectric properties of the host film are expected not to be strongly modified [85]) the (d_{ave}/D) ratio is of the order of 1.7, so that the distance $[d_{ave} - D]$ between adjacent particle surfaces is less than D. In such a case, the deformation fields generated by the individual nanoparticles are expected to overlap, resulting in the transmission of the magnetostrictive strain at long distance. In the case of a uniform distribution of nanoparticles throughout the film, the nanocomposite can be viewed as uniformly deformed along each of the principle directions (X,Y,Z) by the cumulative action of the magnetostrictive nanoparticles. This case will be treated in the next Sections for two possible configurations of the easy axes of nanoparticles; in both cases the nanocomposite is assumed to be submitted to a harmonic driving field directed along the Z-axis (see Equation 1) with the values of frequency and amplitude given in Section 3.

4.2.1 Random distribution of easy axes

Usually, the easy axes of the embedded nanoparticles are randomly oriented with respect to the principle axes of the film. The piezoelectric response of a nanocomposite containing a volume fraction $f_V = 0.1$ of magnetite nanoparticles is studied in detail in the Appendix A.2. The main result of such a treatment is that the polarization vector $\boldsymbol{P}(t)$ is aligned to the magnetic field, with magnitude proportional to the average magnetostrictive strain $\langle \epsilon_3 \rangle$ along the field's direction:

$$\boldsymbol{P}_Z \equiv \boldsymbol{P}_3 = f_V \, G \, \langle \epsilon_3 \rangle \, \boldsymbol{u}_Z \tag{20}$$

where $\boldsymbol{u}_Z$ is the unit vector directed along the Z axis, the brackets denote an average done on all angles between the easy axis and the Z axis, and $G = -8.03 \times 10^{-2}$ C/m^2 for PVDF. The angle-averaged strain $\langle \epsilon_3 \rangle$ is reported in Figure 2, panel *c.1* for a magnetite nanoparticle with $D = 10$ nm (dashed curve in magenta).

As a first approximation, the PVDF film can be compared to a parallel-plate capacitor of finite size immersed in medium of relative permittivity ϵ_r, so that the oscillating electric field inside the film has peak-to-peak value:

$$\Delta E_i \approx \frac{\Delta P_Z}{\epsilon_0 \epsilon_r} = f_V \, |G| \, \frac{|\langle \epsilon_3 \rangle^{MAX} - \langle \epsilon_3 \rangle^{min}|}{\epsilon_0 \epsilon_r} \tag{21}$$

where $\langle \epsilon_3 \rangle^{MAX} \approx 1 \times 10^{-5}$, $\langle \epsilon_3 \rangle^{min} \approx 0$ for the dispersion of S-type magnetite nanoparticles (see Figure 2, panel *c.1*). As it turns out, the electrical field inside the film is $\Delta E_i \approx 9.1 \times 10^3$ V/m when $\epsilon_r \approx 1$ and $f_V = 0.1$. The main magnetostrictive coefficient is $\overline{\alpha}_{ME} \approx 230$ mV/cm/Oe, a value comparable to the results of measurements on similar magnetoelectric polymers [85, 87]. With a film thickness $t_F \approx 200\,\mu$m, the voltage across the film is of the order of 1.8 V, a value larger than the one produced in a PVDF film of comparable thickness submitted to a mechanical stress in an impact testing setup (≈ 0.7 V) [88].

These results have been obtained using a fairly low amplitude of the driving field and a small nanoparticle size; both quantities could be increased without technical

difficulties and without affecting the magnetic regime of the nanoparticles (H_V can be easily increased to 800-1000 Oe and D to 13-14 nm), with an improvement of the voltage. The present results indicate that acting on a PVDF film through a magnetic field instead than by applying a mechanical stress can be an alternate, efficient method to produce a fairly high voltage in the film and an electric field in the neighborhood of the nanocomposite.

In order to assess the potential use of this non-invasive magnetoelectric technique in tissue stimulation, an order-of-magnitude estimate of the electrical fields generated within a medium of relative permittivity ϵ_r can be made by considering the PVDF film as a single electrode applied on the surface of the region to be treated. The electrical value of $E(z)$ at a distance z from the outer surface and along the direction perpendicular to the film's plane can be estimated assuming that the nanocomposite is a parallel-plate capacitor of length 3 cm, width 1.5 cm, thickness 200 μm. In this case one gets [89] $E(z) \approx 90$ V/m on the capacitor's outer surface, while the electrical field inside a medium of mean relative permittivity $\bar{\epsilon}_r$ is equal to $63/\bar{\epsilon}_r$, $33/\bar{\epsilon}_r$, $17/\bar{\epsilon}_r$ V/m at 0.5, 1, 1.5 cm from the nanocomposite-target interface.

4.2.2 Collinear easy axes

An independent way to obtain a better magnetoelectric performance without modifying the magnetic field nor the particle size is to act on the distribution of easy axes of the embedded particles. A significant improvement can be obtained by suitably orienting the easy axes during the formation of the polymer by means of a strong dc magnetic field. The best performance is expected when the common direction of the easy axis is parallel to the applied field.

As discussed in the Appendix A.2, in the collinear case the polarization is simply given by $P_Z(t) = G\, f_V\, \epsilon_Z(t)$, the time behaviour of $\epsilon_Z \equiv \epsilon_{33}\,(\theta = 0)$ being reported in panel *c.1* of Figure 2. Therefore, all electrical quantities, such as ΔE and the voltage across the film, are simply to be multiplied by a factor 3.4 corresponding to the ratio between the peak-to-peak values $\Delta\epsilon_{33}^{(\theta=0)}$ and $\Delta\epsilon_{33}^{(ave)}$ (see Figure 2). In particular, a voltage of about 6.8 V would appear across the PVDF film, a value an order of magnitude larger than the one resulting from the application of an impulsive mechanical stress on a film of same size [88].

5 Conclusion

Two magnetoelectric nanomaterials designed for electrical stimulation of brain and nervous tissues (i.e., core-shell nanoparticles and ME nanocomposites) have been investigated with the aim of optimizing their performance. Both materials exploit the interplay of functional properties which occur in separate components of a composite, biphasic structure. It has been shown that optimizing the ME response requires an accurate knowledge of the magnetostrictive properties of the magnetic nanoparticles as well as of the electro-elastic behaviour of the piezoelectric component. Although the magnitude of magnetostriction is an important parameter, it is by no means the

sole factor determining the magnetostrictive strain produced by the ac magnetic field. As a matter of fact, magnetite nanoparticles have been shown to provide a definitely better magnetostrictive signal than cobalt-ferrite nanoparticles in spite of their lower magnetostriction.

Such a rather counterintuitive result is related to the deep connection existing between magnetostriction and magnetic anisotropy of nanoparticles: a large magnetostriction constant almost always corresponds to a large magnetic anisotropy, i.e., to a high barrier between energy wells of the DWS. The latter brings about a weak magnetic and magnetostrictive response in the presence of an ac field of moderate amplitude (a few hundreds of Oe, as in the case of magneto-electrical stimulation) and a correspondingly weak deformation of the nanoparticle: such an effect overcomes the advantage given by the large magnetostriction constant.

The polarization of a single core-shell nanoparticle whose shell is composed of randomly oriented BTO nanocrystals has been shown to be uniquely related to the magnetostrictive deformation of the core along the direction of the magnetic field. Such a vector produces a periodic electric field both inside and outside the nanoparticle, whose value depends on the permittivity of the dielectric medium which surrounds the ME nanoparticle; a permittivity-independent magnetoelectric coefficient of core-shell particles has been proposed and evaluated in all magnetic regimes and for both ferrite cores.

The ac polarization of an assembly of identical nanoparticles with random easy axes evenly dispersed in a dielectric volume has been shown to be parallel to the applied magnetic field. This interesting result indicates that the direction of the stimulating electric field could be freely varied by merely changing the orientation of the target with respect to the magnetic field (or viceversa), paving the way to directional stimulation of a specific region of the brain.

Another strategy for realizing a non-invasive electrical stimulation of nervous tissues has been investigated by evaluating the magnetoelectric performance of a polymer film containing a uniform dispersion of magnetite nanoparticles. Such a nanocomposite could be used as a single flexible magneto-electrode directly applied at the surface of the target tissue and activated in a wireless fashion without any disturbing circuitry to wear.

It has been shown that the electric field in the film (which can be considered a parallel-plate capacitor of finite size) is parallel to the applied magnetic field; the electric field generated outside the film, whose magnitude depends on the permittivity of the target medium, has been calculated at various distances from the film-tissue interface and shown to be of magnitude suitable to generate electrical stimuli or elicit electrical currents in a resistive medium. The efficiency of the ME film can be increased by a factor of more than three by aligning the easy axes of the nanoparticles by means of a strong dc magnetic field during the formation of the nanocomposite.

In conclusion, the multifunctional properties of nanostructures such as core-shell ME nanoparticles and ME nanocomposite films have the potential for a breakthrough in advanced applications of personalized medicine such as brain cell and nerve stimulation. It has been shown that the inherent complexity of the interplay between magnetic and piezoelastic effects requires an in-depth knowledge of the mechanisms underlying the action of these magnetoelectric nanomaterials. A deeper understanding of physical effects is the key to creating tailor-made magnetoelectric nanostructures eligible for use in *in-vivo* applications.

Supplementary information.

- explicit expression of the mean magnetization vector of a superparamagnetic nanoparticle and of a set of nanoparticles;
- behaviour of the magnetostrictive strains ϵ_{11} and ϵ_{22} for S-type, BH–type, BA-type nanoparticles made of magnetite and cobalt ferrite;
- behaviour of the peak-to-peak value of the magnetostrictive strain along the field's direction as a function of angle θ in magnetite and cobalt ferrite nanoparticles for all magnetic regimes;
- behaviour of the electric polarization along axes 1 an 2 (P_1 and P_2) as a function of time in S-type, BH–type, BA-type nanoparticles made of magnetite and cobalt ferrite.

Conflict of interest

The authors have no relevant financial or non-financial interests to disclose.

Data availability

The data that support the findings of this study are available from the corresponding author upon reasonable request.

Appendix A

A.1 Polarization of a single core-shell nanoparticle

Let us consider a single ME nanoparticle composed of a magnetostrictive core and a piezoelectric shell, as in Figure 1, panel *a*. The reference axes of the magnetic core are labeled $(1, 2, 3)$ as in Section 2. Assuming negligible off-diagonal elements of the magnetostrictive strain tensor and using the Voigt contracted notation, the (6×1) strain vector $\boldsymbol{\epsilon}$ of the magnetic nanoparticle is:

$$\boldsymbol{\epsilon} = \begin{pmatrix} \epsilon_1 \\ \epsilon_2 \\ \epsilon_3 \\ 0 \\ 0 \\ 0 \end{pmatrix} \tag{A1}$$

where $\epsilon_i \equiv \epsilon_{ii}$; $(i = 1, 2, 3)$, the ϵ_{ii}'s being the magnetostrictive strains along the particle axes obtained in Section 3. If the strain is transmitted without significant attenuation from the magnetic core to the surrounding BTO shell, the changes in length along the three axes $(1, 2, 3)$ result in changes along the axes (X, Y, Z) of the cell of each tetragonal BTO nanocrystal. When the (X, Y, Z) axes make the angles α and β with the $(1, 2, 3)$ axes of the magnetic core (Figure A1, panel *a*), the following expressions hold:

$$\begin{aligned} \epsilon_X &= \epsilon_1 \cos\alpha \cos\beta - \epsilon_2 \cos\alpha \sin\beta + \epsilon_3 \sin\alpha \cos\beta \\ \epsilon_Y &= \epsilon_1 \cos\alpha \sin\beta + \epsilon_2 \cos\alpha \cos\beta + \epsilon_3 \sin\alpha \sin\beta \\ \epsilon_Z &= \epsilon_1 \sin\alpha + \epsilon_2 \sin\alpha + \epsilon_3 \cos\alpha \end{aligned} \tag{A2}$$

The (6×1) strain vector in the reference frame of the BTO nanocrystal ($\boldsymbol{\epsilon_L}$) is:

$$\boldsymbol{\epsilon_L} = \begin{pmatrix} \epsilon_X \\ \epsilon_Y \\ \epsilon_Z \\ 0 \\ 0 \\ 0 \end{pmatrix} \tag{A3}$$

The (6×6) stiffness/elastic matrix $[\boldsymbol{C}]$ appropriate to a tetragonal ($P4mm$) BTO single crystal is of the type [90, 91]:

$$[\boldsymbol{C}] = \begin{pmatrix} C_{11} & C_{12} & C_{13} & 0 & 0 & 0 \\ C_{12} & C_{11} & C_{13} & 0 & 0 & 0 \\ C_{13} & C_{13} & C_{33} & 0 & 0 & 0 \\ 0 & 0 & 0 & C_{44} & 0 & 0 \\ 0 & 0 & 0 & 0 & C_{44} & 0 \\ 0 & 0 & 0 & 0 & 0 & C_{66} \end{pmatrix} \tag{A4}$$

where $C_{66} \equiv \frac{1}{2}(C_{11} - C_{12})$. Applying $[\boldsymbol{C}]$ to $\boldsymbol{\epsilon_L}$ results in the (6×1) internal stress vector $\boldsymbol{\sigma}$:

$$\boldsymbol{\sigma} = [\boldsymbol{C}] \cdot \boldsymbol{\epsilon_L} = \begin{pmatrix} C_{11}\epsilon_X + C_{12}\epsilon_Y + C_{13}\epsilon_Z \\ C_{12}\epsilon_X + C_{11}\epsilon_Y + C_{13}\epsilon_Z \\ C_{13}\epsilon_X + C_{13}\epsilon_Y + C_{33}\epsilon_Z \\ 0 \\ 0 \\ 0 \end{pmatrix} \tag{A5}$$

Finally, the (3×1) polarization vector $\boldsymbol{P}$ is obtained by applying to the vector $\boldsymbol{\sigma}$ the 3rd rank direct piezoelectric matrix $[\boldsymbol{d}]$ of dimensions (3×6) appropriate to BTO:

$$[\boldsymbol{d}] = \begin{pmatrix} 0 & 0 & 0 & 0 & d_{15} & 0 \\ 0 & 0 & 0 & d_{15} & 0 & 0 \\ d_{31} & d_{32} & d_{33} & 0 & 0 & 0 \end{pmatrix} \tag{A6}$$

The numerical values of the C_{ij}, d_{ij} matrix elements used in this paper are listed in Table A1, where the stiffness matrix elements C_{ij} and the piezoelectric matrix elements d_{ij} for a BTO single crystal have been obtained by averaging the experimental values reported in Ref. [92].

Table A1 Stiffness matrix elements C_{ij} in BTO single crystals (10^9 N/m^2); piezoelectric matrix elements d_{ij} (10^{-12} C/N); values of the A and B constants defined in Equation A8 (C/m^2).

C_{11} = 242.9
C_{12} = 138.1
C_{13} = 129.4
C_{33} = 157.6
d_{31} = -39.3
d_{33} = 86.7
A = -3.75
B = 3.49

The polarization of a single nanocrystal of BTO in the shell is therefore given by:

$$\boldsymbol{P} = \begin{pmatrix} 0 \\ 0 \\ d_{31}[C_{11}\epsilon_X + C_{12}\epsilon_Y + C_{13}\epsilon_Z] + \\ d_{31}[C_{12}\epsilon_X + C_{11}\epsilon_Y + C_{13}\epsilon_Z] + \\ d_{33}[C_{13}\epsilon_X + C_{13}\epsilon_Y + C_{33}\epsilon_Z] \end{pmatrix} = \begin{pmatrix} 0 \\ 0 \\ A\epsilon_X + A\epsilon_Y + B\epsilon_Z \end{pmatrix} \tag{A7}$$

where:

$$\begin{aligned} A &= d_{31}(C_{11} + C_{12}) + d_{33}C_{13} \\ B &= 2d_{31}C_{13} + d_{33}C_{33} \end{aligned} \tag{A8}$$

The numerical values of the A, B constant are reported in Table A1 for BTO. In the present case, $A < 0$ and $B > |A| > 0$. According to Equation A7, each BTO nanocrystal in the shell acquires a net polarization along the local $Z-$axis. The projections of the $\boldsymbol{P}$ vector on the particle axes are:

$$\begin{aligned} P_1 &= P_Z \sin\alpha \cos\beta \\ P_2 &= P_Z \sin\alpha \sin\beta \\ P_3 &= P_Z \cos\alpha \end{aligned} \tag{A9}$$

The ME particle is polarized along each one of the three reference axes by effect of the considered BTO nanocrystal; the total polarization along the $(1, 2, 3)$ axes is obtained by summing the contributions from all BTO nanocrystals comprised in the shell.

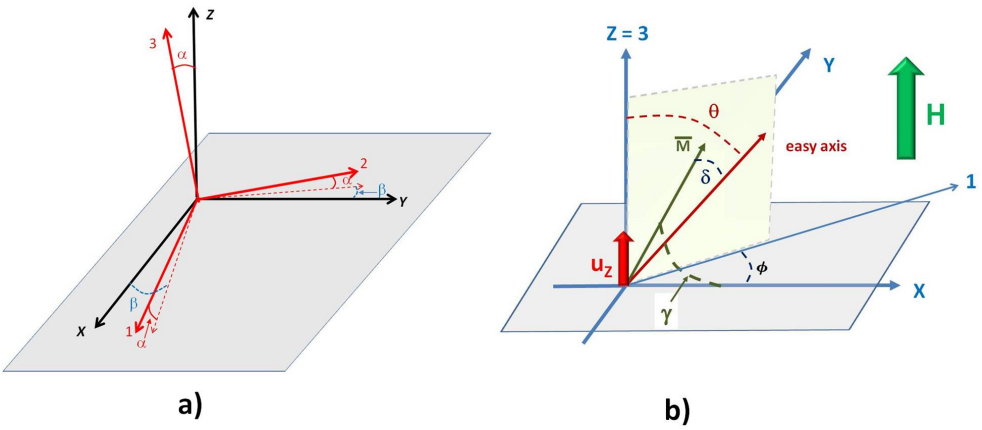

Fig. A1 *a*: (α,β) angles involved in the transformation from the local (X, Y, Z) reference frame of a single BTO nanocrystal in the piezoelectric shell and the (1,2,3) axes of the magnetic core of a ME core-shell nanoparticle; *b*: (θ,ϕ) angles giving the direction of the easy axis of a magnetic nanoparticle with respect to the (XYZ) reference frame fixed to a piezoelectric film; γ is the angle between the direction of the magnetization $\overline{M}$ of the dispersed nanoparticles having in common the same easy-axis direction and the applied field.

In the presence of a large number of nanocrystals whose (X, Y, Z) axes are randomly oriented with respect to the $(1, 2, 3)$ axes, the sum can be substituted by an integral over the (α, β) angles. Taking into account Equations A2 and A7, it can be recognized that all components of the polarization vector defined in Equation A9 are functions of the type $F = F(\alpha, \beta)$ of both angles. As an example, the quantity P_3 can be explicitly written as:

$$\begin{aligned} P_3 = {} & A\left[\epsilon_1 \cos^2\alpha \cos\beta - \epsilon_2 \cos^2\alpha \sin\beta + \epsilon_3 \cos\alpha \sin\alpha \cos\beta\right] + \\ & + A\left[\epsilon_1 \cos^2\alpha \sin\beta + \epsilon_2 \cos^2\alpha \cos\beta + \epsilon_3 \cos\alpha \sin\alpha \sin\beta\right] + \\ & + B\left[\epsilon_1 \sin\alpha \cos\alpha + \epsilon_2 \sin\alpha \cos\alpha + \epsilon_3 \cos^2\alpha\right] \end{aligned} \tag{A10}$$

and similar expressions hold for P_1 and P_2.

The average of $F(\alpha, \beta)$ on the spherical angles is:

$$\overline{F} = \frac{1}{4\pi}\int_{-1}^{1} d(\cos\alpha)\int_{0}^{2\pi} F(\alpha,\beta)\,d\beta. \tag{A11}$$

It can be checked that the integrals of most of the terms of Equation A10 are equal to zero; the only surviving term is:

$$\overline{P}_3 = \frac{1}{2}B\epsilon_3\int_{-1}^{1}\cos^2\alpha\ d(\cos\alpha) = \frac{1}{3}B\epsilon_3. \tag{A12}$$

In a similar way, it can be easily shown that:

$$\overline{P_1} = \overline{P_2} = \frac{1}{3}A\epsilon_3, \tag{A13}$$

Note that ϵ_3 is the variation of the magnetic core's length along the field direction, which is still a function of the angle θ between the easy axis and the magnetic field direction (see panel *b* of Figures 2, 3 and 4). It can be concluded that each nanoparticle carries in general a nonzero polarization along each of the directions corresponding to the (1,2,3) axes. The magnetoelectric effects of core-shell nanoparticles are studied in Section 4.1.

A.2 Polarization of a PVDF film containing magnetite nanoparticles

A set of superparamagnetic nanoparticles of magnetite with $D = 10$ nm are evenly dispersed with volume fraction $f_V = 0.a$ in a rectangular PVDF film; their easy axes are randomly directed with respect to the reference axes of the film.

In the (X,Y,Z) reference frame of the PVDF film, the easy-axis direction of each nanoparticle is characterized by the polar angles (θ,ϕ), as sketched in in Figure A1, panel *b*. The Z-axis is coincident with axis 3 of the particle frame; the magnetic field induces the rotation of the mean magnetization vector $\overline{\boldsymbol{M}}$ (see the Supplementary Information) by the angle δ in the $(1,3)$ plane. The angle between $\overline{\boldsymbol{M}}$ and the Z-axis is $(\theta-\delta)$, so that according to Equation 2:

$$\epsilon_Z \equiv \epsilon_{33} = \frac{3}{2}\lambda_s\left(\frac{\overline{M}}{M_s}\right)^2\left[\cos^2(\theta-\delta)-\frac{1}{3}\right] \tag{A14}$$

The magnetostrictive strain along the X-axis. ϵ_X, is given by the expression:

$$\epsilon_X = \frac{3}{2}\lambda_s\left(\frac{\overline{M}}{M_s}\right)^2\left[\cos^2\gamma-\frac{1}{3}\right] \tag{A15}$$

where γ is the angle between the magnetization and the X-axis (Figure A1b). Using the standard expression of the cosine of the angle γ between two directions in space characterized by polar angles (θ_1,ϕ_1) and (θ_2,ϕ_2),

$$\cos\gamma = \cos\theta_1\cos\theta_2 + \sin\theta_1\sin\theta_2\cos(\phi_1-\phi_2) \tag{A16}$$

and taking into account that in the examined case: $\theta_1 = (\theta-\delta); \phi_1 = \phi; \theta_2 = \pi/2, \phi_2 = 0$, one gets:

$$\epsilon_X = \frac{3}{2}\lambda_s \left(\frac{\overline{M}}{M_s}\right)^2 \left[\sin^2(\theta-\delta)\cos^2\phi - \frac{1}{3}\right] \tag{A17}$$

In a similar way it can be easily shown that:

$$\epsilon_Y = \frac{3}{2}\lambda_s \left(\frac{\overline{M}}{M_s}\right)^2 \left[\sin^2(\theta-\delta)\sin^2\phi - \frac{1}{3}\right] \tag{A18}$$

In a film containing nanoparticles with random easy axes, these strains are to be averaged over the (θ, ϕ) angles. Let do the average on ϕ first: this angle is evenly distributed between 0 and π and appears in the expressions of ϵ_X, ϵ_Y only. Therefore, the average over ϕ leaves ϵ_Z unchanged: $\overline{\epsilon}_Z \equiv \epsilon_Z$, whereas:

$$\begin{aligned}
\overline{\epsilon}_X &= \frac{3}{2}\lambda_s \left(\frac{\overline{M}}{M_s}\right)^2 \left[\sin^2(\theta-\delta)\overline{\cos^2\phi} - \frac{1}{3}\right] \\
\overline{\epsilon}_Y &= \frac{3}{2}\lambda_s \left(\frac{\overline{M}}{M_s}\right)^2 \left[\sin^2(\theta-\delta)\overline{\sin^2\phi} - \frac{1}{3}\right]
\end{aligned} \tag{A19}$$

Using $\overline{\cos^2\phi} = \overline{\sin^2\phi} = 1/2$, it can be immediately observed that $\overline{\epsilon}_X = \overline{\epsilon}_Y = -\frac{1}{2}\epsilon_Z$, as indeed expected. The average of ϵ_Z over the angle θ (which takes all values between 0 and π) is:

$$\langle \epsilon_Z \rangle = \frac{1}{2}\int_0^\pi \epsilon_Z(\theta)\, \sin\theta\, d\theta \tag{A20}$$

Therefore, the strains generated by embedded nanoparticles with random easy axes along the three principle directions of the film are $\langle \overline{\epsilon}_Z \rangle$ and $\langle \overline{\epsilon}_X \rangle = \langle \overline{\epsilon}_Y \rangle = -\frac{1}{2}\langle \epsilon_Z \rangle$, so that only one independent quantity is needed to fully characterize the (6×1) vector $\boldsymbol{\epsilon_P}$ in the piezoelectric film:

$$\boldsymbol{\epsilon_P} = \begin{pmatrix} -\frac{1}{2}\langle \epsilon_Z \rangle \\ -\frac{1}{2}\langle \epsilon_Z \rangle \\ \langle \epsilon_Z \rangle \\ 0 \\ 0 \\ 0 \end{pmatrix} \tag{A21}$$

The polarization of the PVDF film can be obtained along the same lines discussed in the Appendix A.1, i.e., by forming the (6×1) stress vector $\boldsymbol{\sigma_P} = [\boldsymbol{C}] \cdot \boldsymbol{\epsilon_P}$ and the (3×1) polarization vector $\boldsymbol{P} = [\boldsymbol{d}] \cdot \boldsymbol{\sigma_P}$, using appropriate values for the elements of the stiffness constant $[\boldsymbol{C}]$ [93] and of the direct piezoelectric matrix $[\boldsymbol{d}]$ (the values of the matrix elements relevant to our calculations are reported in Table A2).

As in the case of core-shell structures, the polarization vector is characterized by one nonzero component:

Table A2 Stiffness matrix elements C_{ij} in PVDF (10^9 N/m^2) calculated from the elastic constants reported in Ref. [82]; piezoelectric matrix elements d_{ij} (10^{-12} C/N) taken from Ref. [82]; values of the G constant defined in Equation A23 (in C/m^2).

$C_{11} = 6.43$
$C_{12} = 4.25$
$d_{31} = 18$
$d_{32} = 5$
d_{33} = -26
$G = -8.03 \times 10^{-2}$

$$\boldsymbol{P} = \begin{pmatrix} 0 \\ 0 \\ G\langle \epsilon_Z \rangle \end{pmatrix} \tag{A22}$$

where the constant G (which only depends on the piezoelectric film) is given by:

$$G = \left(d_{33} - \frac{d_{31} + d_{32}}{2} \right) \left[C_{11} - C_{12} \right] \tag{A23}$$

and takes the value $G = -8.03 \times 10^{-2}$ C/m^2 in PVDF.

Finally, when the easy axes are collinear and directed along the Z-axis, both θ and δ are equal to zero and there is no need to perform the average over the polar angles, so that the three magnetostrictive strains reduce to:

$$\begin{aligned} \epsilon_Z &= \lambda_s \left(\frac{\overline{M}}{M_s} \right)^2 \\ \epsilon_X &= -\frac{\epsilon_Z}{2} \\ \epsilon_Y &= -\frac{\epsilon_Z}{2}. \end{aligned} \tag{A24}$$

References

[1] Nunez, P.L., Srinivasan, R.: Electric Fields of the Brain: the Neurophysics of EEG. Oxford University Press, USA, Oxford (2006)

[2] Bensmaia, S.J., Miller, L.E.: Restoring sensorimotor function through intracortical interfaces: progress and looming challenges. Nature Reviews Neuroscience **15**(5), 313–325 (2014)

[3] Pesaran, B., Vinck, M., Einevoll, G.T., Sirota, A., Fries, P., Siegel, M., Truccolo, W., Schroeder, C.E., Srinivasan, R.: Investigating large-scale brain dynamics

using field potential recordings: analysis and interpretation. Nature neuroscience **21**(7), 903–919 (2018)

[4] Wichmann, T., DeLong, M.R.: Deep brain stimulation for neurologic and neuropsychiatric disorders. Neuron **52**(1), 197–204 (2006)

[5] Montgomery Jr, E.B., Gale, J.T.: Mechanisms of action of deep brain stimulation (dbs). Neuroscience & Biobehavioral Reviews **32**(3), 388–407 (2008)

[6] Foutz, T.J., Wong, M.: Brain stimulation treatments in epilepsy: basic mechanisms and clinical advances. biomedical journal **45**(1), 27–37 (2022)

[7] Vissani, M., Isaias, I.U., Mazzoni, A.: Deep brain stimulation: a review of the open neural engineering challenges. Journal of neural engineering **17**(5), 051002 (2020)

[8] Francis, J.T., Gluckman, B.J., Schiff, S.J.: Sensitivity of neurons to weak electric fields. Journal of Neuroscience **23**(19), 7255–7261 (2003)

[9] Adair, D., Truong, D., Esmaeilpour, Z., Gebodh, N., Borges, H., Ho, L., Bremner, J.D., Badran, B.W., Napadow, V., Clark, V.P., *et al.*: Electrical stimulation of cranial nerves in cognition and disease. Brain stimulation **13**(3), 717–750 (2020)

[10] Allen, C.B., Williamson, T.K., Norwood, S.M., Gupta, A.: Do electrical stimulation devices reduce pain and improve function?—a comparative review. Pain and Therapy **12**(6), 1339–1354 (2023)

[11] Kumari, P., Wunderlich, H., Milojkovic, A., López, J.E., Fossati, A., Jahanshahi, A., Kozielski, K.: Multiscale modeling of magnetoelectric nanoparticles for the analysis of spatially selective neural stimulation. Advanced healthcare materials, 2302871 (2024)

[12] Kim, E., Kim, S., Kwon, Y.W., Seo, H., Kim, M., Chung, W.G., Park, W., Song, H., Lee, D.H., Lee, J., *et al.*: Electrical stimulation for therapeutic approach. Interdisciplinary Medicine **1**(2), 20230003 (2023)

[13] Siddiqi, S.H., Khosravani, S., Rolston, J.D., Fox, M.D.: The future of brain circuit-targeted therapeutics. Neuropsychopharmacology **49**(1), 179–188 (2024)

[14] Johnson, M.: Transcutaneous electrical nerve stimulation: mechanisms, clinical application and evidence. Reviews in pain **1**(1), 7–11 (2007)

[15] Kashyap, N., Baranwal, V.K., Basumatary, B., Bansal, R., Sahani, A.: A systematic review on muscle stimulation techniques. IETE Technical Review **40**(1), 76–89 (2023)

[16] Ong Sio, L.C., Hom, B., Garg, S., Abd-Elsayed, A.: Mechanism of action of peripheral nerve stimulation for chronic pain: a narrative review. International

Journal of Molecular Sciences **24**(5), 4540 (2023)

[17] Trout, M.A., Harrison, A.T., Brinton, M.R., George, J.A.: A portable, programmable, multichannel stimulator with high compliance voltage for noninvasive neural stimulation of motor and sensory nerves in humans. Scientific Reports **13**(1), 3469 (2023)

[18] Thomas, C., Truong, D.Q., Lee, K., Deblieck, C., Androulakis, X.M., Datta, A.: Determination of current flow induced by transcutaneous electrical nerve stimulation for the treatment of migraine: Potential for optimization. Frontiers in Pain Research **2**, 753454 (2021)

[19] Singer, A., Dutta, S., Lewis, E., Chen, Z., Chen, J.C., Verma, N., Avants, B., Feldman, A.K., O'Malley, J., Beierlein, M., *et al.*: Magnetoelectric materials for miniature, wireless neural stimulation at therapeutic frequencies. Neuron **107**(4), 631–643 (2020)

[20] Davidson, B., Milosevic, L., Kondrataviciute, L., Kalia, L.V., Kalia, S.K.: Neuroscience fundamentals relevant to neuromodulation: Neurobiology of deep brain stimulation in parkinson's disease. Neurotherapeutics **21**(3), 00348 (2024)

[21] Krauss, J.K., Lipsman, N., Aziz, T., Boutet, A., Brown, P., Chang, J.W., Davidson, B., Grill, W.M., Hariz, M.I., Horn, A., *et al.*: Technology of deep brain stimulation: current status and future directions. Nature Reviews Neurology **17**(2), 75–87 (2021)

[22] Hariz, M.I.: Complications of deep brain stimulation surgery. Movement disorders: official journal of the Movement Disorder Society **17**(S3), 162–166 (2002)

[23] Sarica, C., Iorio-Morin, C., Aguirre-Padilla, D.H., Najjar, A., Paff, M., Fomenko, A., Yamamoto, K., Zemmar, A., Lipsman, N., Ibrahim, G.M., *et al.*: Implantable pulse generators for deep brain stimulation: challenges, complications, and strategies for practicality and longevity. Frontiers in Human Neuroscience **15**, 708481 (2021)

[24] Polania, R., Nitsche, M.A., Ruff, C.C.: Studying and modifying brain function with non-invasive brain stimulation. Nature neuroscience **21**(2), 174–187 (2018)

[25] Krause, M.R., Vieira, P.G., Pack, C.C.: Transcranial electrical stimulation: How can a simple conductor orchestrate complex brain activity? Plos Biology **21**(1), 3001973 (2023)

[26] Yang, D., Shin, Y.-I., Hong, K.-S.: Systemic review on transcranial electrical stimulation parameters and eeg/fnirs features for brain diseases. Frontiers in Neuroscience **15**, 629323 (2021)

[27] Wu, L., Liu, T., Wang, J.: Improving the effect of transcranial alternating current

stimulation (tacs): A systematic review. Frontiers in Human Neuroscience **15**, 652393 (2021)

[28] Yue, K., Guduru, R., Hong, J., Liang, P., Nair, M., Khizroev, S.: Magneto-electric nano-particles for non-invasive brain stimulation. PLOS One **7**(9), 44040 (2012)

[29] Kozielski, K.L., Jahanshahi, A., Gilbert, H.B., Yu, Y., Erin, Ö., Francisco, D., Alosaimi, F., Temel, Y., Sitti, M.: Nonresonant powering of injectable nanoelectrodes enables wireless deep brain stimulation in freely moving mice. Science advances **7**(3), 4189 (2021)

[30] Nguyen, T., Gao, J., Wang, P., Nagesetti, A., Andrews, P., Masood, S., Vriesman, Z., Liang, P., Khizroev, S., Jin, X.: In vivo wireless brain stimulation via non-invasive and targeted delivery of magnetoelectric nanoparticles. Neurotherapeutics **18**(3), 2091–2106 (2021)

[31] Colombo, E., Feyen, P., Antognazza, M.R., Lanzani, G., Benfenati, F.: Nanoparticles: a challenging vehicle for neural stimulation. Frontiers in neuroscience **10**, 183159 (2016)

[32] Sun, L., Liu, H., Ye, Y., Lei, Y., Islam, R., Tan, S., Tong, R., Miao, Y.-B., Cai, L.: Smart nanoparticles for cancer therapy. Signal transduction and targeted therapy **8**(1), 418 (2023)

[33] Roet, M., Hescham, S.-A., Jahanshahi, A., Rutten, B.P., Anikeeva, P.O., Temel, Y.: Progress in neuromodulation of the brain: A role for magnetic nanoparticles? Progress in neurobiology **177**, 1–14 (2019)

[34] Dante, S., Petrelli, A., Petrini, E.M., Marotta, R., Maccione, A., Alabastri, A., Quarta, A., De Donato, F., Ravasenga, T., Sathya, A., *et al.*: Selective targeting of neurons with inorganic nanoparticles: revealing the crucial role of nanoparticle surface charge. ACS nano **11**(7), 6630–6640 (2017)

[35] Apu, E.H., Nafiujjaman, M., Sandeep, S., Makela, A.V., Khaleghi, A., Vainio, S., Contag, C.H., Li, J., Balasingham, I., Kim, T., *et al.*: Biomedical applications of multifunctional magnetoelectric nanoparticles. Materials Chemistry Frontiers **6**(11), 1368–1390 (2022)

[36] Wang, B., He, X., Zhang, Z., Zhao, Y., Feng, W.: Metabolism of nanomaterials in vivo: blood circulation and organ clearance. Accounts of chemical research **46**(3), 761–769 (2013)

[37] Guduru, R., Liang, P., Hong, J., Rodzinski, A., Hadjikhani, A., Horstmyer, J., Levister, E., Khizroev, S.: Magnetoelectric 'spin'on stimulating the brain. Nanomedicine **10**(13), 2051–2061 (2015)

[38] Rao, B.N., Kaviraj, P., Vaibavi, S., Kumar, A., Bajpai, S.K., Arockiarajan, A.:

Investigation of magnetoelectric properties and biocompatibility of cofe2o4-batio3 core-shell nanoparticles for biomedical applications. Journal of Applied Physics **122**(16) (2017)

[39] Zhang, Y., Wu, X., Ding, J., Su, B., Chen, Z., Xiao, Z., Wu, C., Wei, D., Sun, J., Luo, F., *et al.*: Wireless-powering deep brain stimulation platform based on 1d-structured magnetoelectric nanochains applied in antiepilepsy treatment. ACS nano **17**(16), 15796–15809 (2023)

[40] Eerenstein, W., Mathur, N., Scott, J.F.: Multiferroic and magnetoelectric materials. nature **442**(7104), 759–765 (2006)

[41] Lawes, G., Srinivasan, G.: Introduction to magnetoelectric coupling and multiferroic films. Journal of Physics D: Applied Physics **44**(24), 243001 (2011)

[42] Shrimali, V.G., Gadani, K., Jashi, A.D., Asokan, K., Solanki, P.S., Shah, N.A.: Role of defects in multiferroic nanoparticles. In: Kumar, V., Som, S., Vishal, S., Swat, H. (eds.) Metal Oxide Defects Fundamentals, Design, Development and Applications, pp. 161–189. Elsevier, Amsterdam (2023). Chap. 6

[43] Smith, I.T., Zhang, E., Yildirim, Y.A., Campos, M.A., Abdel-Mottaleb, M., Yildirim, B., Ramezani, Z., Andre, V.L., Scott-Vandeusen, A., Liang, P., *et al.*: Nanomedicine and nanobiotechnology applications of magnetoelectric nanoparticles. Wiley interdisciplinary reviews: nanomedicine and Nanobiotechnology **15**(2), 1849 (2023)

[44] Narayanan, R.P., Khaleghi, A., Veletić, M., Balasingham, I.: Multiphysics simulation of magnetoelectric micro core-shells for wireless cellular stimulation therapy via magnetic temporal interference. Plos one **19**(1), 0297114 (2024)

[45] Sebastian, V.: Design of Magnetostrictive Nanoparticles for Magnetoelectric Composites. In: Lanceros-Méndez, S., Martins, P. (eds.) Magnetoelectric Polymer-Based Composites: Fundamentals and Applications. Wiley-VCH Verlag GmbH & Co. KGaA, Weinheim, Germany (2017). Chap. 5

[46] Marrella, A., Suarato, G., Fiocchi, S., Chiaramello, E., Bonato, M., Parazzini, M., Ravazzani, P.: Magnetoelectric nanoparticles shape modulates their electrical output. Frontiers in Bioengineering and Biotechnology **11**, 1219777 (2023)

[47] Betal, S., Shrestha, B., Dutta, M., Cotica, L.F., Khachatryan, E., Nash, K., Tang, L., Bhalla, A.S., Guo, R.: Magneto-elasto-electroporation (meep): In-vitro visualization and numerical characteristics. Scientific reports **6**(1), 32019 (2016)

[48] Fiocchi, S., Chiaramello, E., Marrella, A., Suarato, G., Bonato, M., Parazzini, M., Ravazzani, P.: Modeling of core-shell magneto-electric nanoparticles for biomedical applications: Effect of composition, dimension, and magnetic field features on magnetoelectric response. PloS one **17**(9), 0274676 (2022)

[49] Song, H., Listyawan, M.A., Ryu, J.: Core–shell magnetoelectric nanoparticles: materials, synthesis, magnetoelectricity, and applications. In: Actuators, vol. 11, p. 380 (2022). MDPI

[50] Zhang, Y., Chen, S., Xiao, Z., Liu, X., Wu, C., Wu, K., Liu, A., Wei, D., Sun, J., Zhou, L., *et al.*: Magnetoelectric nanoparticles incorporated biomimetic matrix for wireless electrical stimulation and nerve regeneration. Advanced Healthcare Materials **10**(16), 2100695 (2021)

[51] Wang, P., Zhang, E., Toledo, D., Smith, I.T., Navarrete, B., Furman, N., Hernandez, A.F., Telusma, M., McDaniel, D., Liang, P., *et al.*: Colossal magnetoelectric effect in core–shell magnetoelectric nanoparticles. Nano letters **20**(8), 5765–5772 (2020)

[52] Reaz, M., Haque, A., Ghosh, K.: Synthesis, characterization, and optimization of magnetoelectric batio3–iron oxide core–shell nanoparticles. Nanomaterials **10**(3), 563 (2020)

[53] Chaudhuri, A., Mandal, K.: Large magnetoelectric properties in cofe2o4: Batio3 core–shell nanocomposites. Journal of Magnetism and Magnetic Materials **377**, 441–445 (2015)

[54] Chiaramello, E., Fiocchi, S., Bonato, M., Marrella, A., Suarato, G., Parazzini, M., Ravazzani, P.: Magnetoelectric nanoparticles: evaluating stimulation feasibility of the possible next generation approach for deep brain stimulation. IEEE Access **10**, 124884–124893 (2022)

[55] Zhang, E., Abdel-Mottaleb, M., Liang, P., Navarrete, B., Yildirim, Y.A., Campos, M.A., Smith, I., Wang, P., Yildirim, B., Yang, L., *et al.*: Magnetic-field-synchronized wireless modulation of neural activity by magnetoelectric nanoparticles. Brain stimulation **15**(6), 1451–1462 (2022)

[56] Guo, H., Baker, A., Guo, J., Randall, C.: Protocol for ultralow-temperature ceramic sintering: an integration of nanotechnology and the cold sintering process, ACS Nano 10 (2016) 10606–10614

[57] Cullity, B.D., Graham, C.D.: Introduction to Magnetic Materials. John Wiley & Sons, Hoboken, New Jersey (2011)

[58] Knobel, M., Nunes, W., Socolovsky, L., De Biasi, E., Vargas, J., Denardin, J.: Superparamagnetism and other magnetic features in granular materials: a review on ideal and real systems. Journal of nanoscience and nanotechnology **8**(6), 2836–2857 (2008)

[59] Buschow, K.J.: Handbook of Magnetic Materials. Elsevier, Amsterdam, The Netherlands (2003)

[60] Liu, J., Wu, K., Wang, J.-P.: Magnetic properties of cubic feco nanoparticles with anisotropic long chain structure. AIP Advances **6**(5) (2016)

[61] Skandalakis, G.P., Rivera, D.R., Rizea, C.D., Bouras, A., Jesu Raj, J.G., Bozec, D., Hadjipanayis, C.G.: Hyperthermia treatment advances for brain tumors. International Journal of Hyperthermia **37**(2), 3–19 (2020)

[62] Barrera, G., Allia, P., Tiberto, P.: Dipolar interactions among magnetite nanoparticles for magnetic hyperthermia: A rate-equation approach. Nanoscale **13**(7), 4103–4121 (2021)

[63] Perigo, E.A., Hemery, G., Sandre, O., Ortega, D., Garaio, E., Plazaola, F., Teran, F.J.: Fundamentals and advances in magnetic hyperthermia. Applied Physics Reviews **2**(4) (2015)

[64] Dutz, S., Kettering, M., Hilger, I., Müller, R., Zeisberger, M.: Magnetic multicore nanoparticles for hyperthermia—influence of particle immobilization in tumour tissue on magnetic properties. Nanotechnology **22**(26), 265102 (2011)

[65] Birdno, M.J., Grill, W.M.: Mechanisms of deep brain stimulation in movement disorders as revealed by changes in stimulus frequency. Neurotherapeutics **5**, 14–25 (2008)

[66] Chikazumi, S., Graham, C.D.: Physics of Ferromagnetism vol. 94. Oxford university press, Oxford (1997)

[67] Allia, P., Barrera, G., Tiberto, P.: Linearized rate-equation approach for double-well systems: Cooling-and temperature-dependent low-field magnetization of magnetic nanoparticles. Physical Review B **98**(13), 134423 (2018)

[68] Allia, P., Barrera, G., Tiberto, P.: Hysteresis effects in magnetic nanoparticles: A simplified rate-equation approach. Journal of Magnetism and Magnetic Materials **496**, 165927 (2020)

[69] Chalifour, A.R., Davidson, J.C., Anderson, N.R., Crawford, T.M., Livesey, K.L.: Magnetic relaxation time for an ensemble of nanoparticles with randomly aligned easy axes: A simple expression. Physical Review B **104**(9), 094433 (2021)

[70] Ota, S., Takemura, Y.: Characterization of néel and brownian relaxations isolated from complex dynamics influenced by dipole interactions in magnetic nanoparticles. The Journal of Physical Chemistry C **123**(47), 28859–28866 (2019)

[71] Barrera, G., Allia, P., Tiberto, P.: Magnetic nanoparticles in square-wave fields for breakthrough performance in hyperthermia and magnetic particle imaging. Scientific Reports **14**(1), 10704 (2024)

[72] Barrera, G., Allia, P., Tiberto, P.: Magnetization dynamics of superparamagnetic

nanoparticles for magnetic particle spectroscopy and imaging. Physical Review Applied **18**(2), 024077 (2022)

[73] Amaral, R., Lemos, N.: A dipole in a dielectric: Intriguing results and shape dependence of the distant electric field. American Journal of Physics **71**(4), 392–396 (2003)

[74] Tamm, I.E.: Fundamentals of the Theory of Electricity, (1979)

[75] Duong, G.V., Grössinger, R., Schoenhart, M., Bueno-Basques, D.: The lock-in technique for studying magnetoelectric effect. Journal of Magnetism and Magnetic Materials **316**(2), 390–393 (2007)

[76] Willard, M., Kurihara, L., Carpenter, E., Calvin, S., Harris, V.: Chemically prepared magnetic nanoparticles. International materials reviews **49**(3-4), 125–170 (2004)

[77] https://itis.swiss/virtual-population/tissue-properties/database/dielectric-properties. https://itis.swiss/virtual-population/tissue-properties/database/dielectric-properties

[78] Zimmermann, J., Rienen, U.: Ambiguity in the interpretation of the low-frequency dielectric properties of biological tissues. Bioelectrochemistry **140**, 107773 (2021)

[79] Lee, S.W., Fallegger, F., Casse, B.D., Fried, S.I.: Implantable microcoils for intracortical magnetic stimulation. Science advances **2**(12), 1600889 (2016)

[80] Genchi, G.G., Marino, A., Rocca, A., Mattoli, V., Ciofani, G.: Barium titanate nanoparticles: promising multitasking vectors in nanomedicine. Nanotechnology **27**(23), 232001 (2016)

[81] Dallaev, R., Pisarenko, T., Sobola, D., Orudzhev, F., Ramazanov, S., Trčka, T.: Brief review of pvdf properties and applications potential. Polymers **14**(22), 4793 (2022)

[82] Wu, T., Jin, H., Dong, S., Xuan, W., Xu, H., Lu, L., Fang, Z., Huang, S., Tao, X., Shi, L., *et al.*: A flexible film bulk acoustic resonator based on β-phase polyvinylidene fluoride polymer. Sensors **20**(5), 1346 (2020)

[83] Kalimuldina, G., Turdakyn, N., Abay, I., Medeubayev, A., Nurpeissova, A., Adair, D., Bakenov, Z.: A review of piezoelectric pvdf film by electrospinning and its applications. Sensors **20**(18), 5214 (2020)

[84] Hu, H., Han, Y., Song, A., Chen, S., Wang, C., Wang, Z.: A finger-shaped tactile sensor for fabric surfaces evaluation by 2-dimensional active sliding touch. Sensors **14**(3), 4899–4913 (2014)

[85] Martins, P., Lasheras, A., Gutiérrez, J., Barandiarán, J.M., Orue, I., Lanceros-Méndez, S.: Optimizing piezoelectric and magnetoelectric responses on cofe2o4/p (vdf-trfe) nanocomposites. Journal of Physics D: Applied Physics **44**(49), 495303 (2011)

[86] Gonçalves, R., Larrea, A., Sebastian, M., Sebastian, V., Martins, P., Lanceros-Mendez, S.: Synthesis and size dependent magnetostrictive response of ferrite nanoparticles and their application in magnetoelectric polymer-based multiferroic sensors. Journal of Materials Chemistry C **4**(45), 10701–10706 (2016)

[87] Zhang, J., Dai, J., So, L., Sun, C., Lo, C., Or, S.W., Chan, H.: The effect of magnetic nanoparticles on the morphology, ferroelectric, and magnetoelectric behaviors of cfo/p (vdf-trfe) 0–3 nanocomposites. Journal of Applied Physics **105**(5) (2009)

[88] Mokhtari, F., Shamshirsaz, M., Latifi, M., Asadi, S.: Comparative evaluation of piezoelectric response of electrospun pvdf (polyvinilydine fluoride) nanofiber with various additives for energy scavenging application. The Journal of the Textile Institute **108**(6), 906–914 (2017)

[89] Parker, G.: Electric field outside a parallel plate capacitor. American Journal of Physics **70**(5), 502–507 (2002)

[90] Bechmann, R.: Elastic, piezoelectric, and dielectric constants of polarized barium titanate ceramics and some applications of the piezoelectric equations. The Journal of the Acoustical Society of America **28**(3), 347–350 (1956)

[91] Electrical, I., Engineers, E.: ANSI/IEEE Std 176-1987: IEEE Standard on Piezoelectricity. IEEE, ??? (1988)

[92] Li, Z., Chan, S.-K., Grimsditch, M., Zouboulis, E.: The elastic and electromechanical properties of tetragonal batio3 single crystals. Journal of Applied Physics **70**(12), 7327–7332 (1991)

[93] Theodorou, D.N., Suter, U.W.: Atomistic modeling of mechanical properties of polymeric glasses. Macromolecules **19**(1), 139–154 (1986)